1 **Morpho-functional characterisation of cœlomocytes in the**

2 **aquacultivated sea cucumber _Holothuria scabra_: from cell diversity**

3 **to transcriptomic immune response**

4 Noé Wambreuse[1,2], Guillaume Caulier[1,2], Igor Eeckhaut[1,2], Laura Borrello[1], Fabrice

5 Bureau[3], Laurence Fievez[3], Jérôme Delroisse[1]

7 [1] Biology of Marine Organisms and Biomimetics Unit, Research Institute for

8 Biosciences, University of Mons (UMONS), 7000 Mons, Belgium

9 [2] Belaza Marine Station (IH.SM-UMONS-ULIEGE), Toliara 601, Madagascar

10 [3] Laboratory of Cellular and Molecular Immunology, GIGA Research,

11 University of Liège, 4000 Liège, Belgium

12 * Corresponding author. Email: noe.wambreuse@umons.ac.be. Postal address: 6,

13 Avenue du Champ de Mars, 7000 Mons, Belgium

14

15

16

17

18

19

1

Graphical abstract

Abstract

Holothuria scabra is one of the most valuable species of sea cucumber owing to its exploitation as a seafood product. This study aims to describe the main molecular and cellular actors in the immunology of the holothuroid *H. scabra*. First of all, a detailed description of the immune cells – the cœlomocytes – is provided, highlighting five main cell types including phagocytes, small round cells (SRCs), spherulocytes, fusiform cells, and crystal cells, with a further five subtypes identified using transmission electron microscopy. Cœlomocyte aggregates were also described morphologically, yielding two main types, one comprising three successive maturation stages. A comparison of the concentration and proportion of cell populations was carried out between the two main body fluids, namely the hydrovascular fluid of the Polian vesicle (HF) and the perivisceral fluid of the general cavity (PF), and no clear relation could be revealed. Next, the cœlomocyte immune response was studied 24 hours after lipopolysaccharide (LPS) injections. Firstly, the fluctuation in cell populations was assessed, and despite a high inter-individual variability, it shows a decrease in the phagocyte proportion and an increase in the SRC proportion. Secondly, the differential

2

40 gene expression of PF cœlomocytes was studied by *de novo* RNA-sequencing

41 between LPS-injected and control-injected individuals: 945 genes were differentially

42 expressed, including 673 up-regulated and 272 down-regulated in the LPS-injected

43 individuals. Among these genes, 80 had a presumed function in immunity based on

44 their annotation, covering a wide range of immune mechanisms. Overall, this study

45 reveals a complex immune system at both molecular and cellular levels and constitutes

46 a baseline reference on *H. scabra* immunity, which may be useful for the development

47 of sustainable aquaculture and provides valuable data for comparative immunology.

48 ## 1. <u>Introduction</u>

49 Sea cucumbers (*i.e.* holothuroids) are benthic marine invertebrates belonging to the

50 phylum Echinodermata. Some species are crucial for marine ecosystems by acting as

51 keystone bioturbators and around 70 species have also a high economic value owing

52 to their exploitation in Asian gastronomy and traditional pharmacopoeia [1]. *Holothuria*

53 *scabra*, a tropical sea cucumber living in the shallow seabed of Indo-Pacific waters, is

54 among the most prized species [2]. In recent decades, its overexploitation has led to

55 significant declines in wild stocks [1,2]. While conservation actions and the emergence

56 of sustainable aquacultures offer good hopes for the future of this endangered species,

57 *H. scabra* is subject to epidemic diseases that lead to significant mortalities, both in the

58 wild and in aquaculture facilities [2,3]. To better understand the development of these

59 diseases in this species, and more broadly in sea cucumbers, it is necessary to gain

60 knowledge about their immune system that remains understudied.

61 The immunity of echinoderms is mediated by free-circulating cells, the cœlomocytes,

62 that are involved in numerous functions including phagocytosis, encapsulation, and

63 wound healing [4]. These particular cells can be found in a wide variety of tissues but

3

64   are particularly abundant within the perivisceral fluid from the general cavity (PF) and

65   the hydrovascular fluid from the water vascular (*i.e.* ambulacrarian) system (HF). In the

66   last decades, numerous studies have described various cœlomocyte types in different

67   species using a large variety of methods (*e.g.* [5–7]). Although some cell types are

68   common to different species, many different designations/synonyms exist in the

69   literature which complicate the establishment of a generalised coelomocyte

70   classification. The most accepted ones comprise six to seven cell types including

71   phagocytes, spherulocytes, vibratile cells, hemocytes, progenitor cells, crystal cells

72   and fusiform cells [4,8]. In *H. scabra*, little information exists about cœlomocytes and,

73   to our knowledge, only Prompoon et al. [9] have contributed to the description of their

74   cell types based on a flow cytometry approach combined with lectin labelling. While

75   this study provided a basic description of cœlomocyte diversity in *H. scabra*, their

76   functional characterisation requires further investigations.

77   The immune response also involves the expression of a large number of genes coding

78   for different cellular activity regulators and humoral factors. In recent years, RNA-

79   sequencing (RNA-seq) has become a prominent tool for identifying differentially

80   expressed genes (DEGs) following various stresses [10]. In sea cucumbers, and

81   especially in the species *Apostichopus japonicus*, RNA-seq has been notably

82   employed to characterise the immune response of cœlomocytes to different

83   immunological stress including exposure to *Vibrio splendidus*, a common pathogen

84   bacteria of sea cucumbers [11], or lipopolysaccharide (LPS) [12], an endotoxin

85   characteristic of Gram-negative bacteria that is commonly used to generate an immune

86   response. While these few studies all point to great complexity in the immune response

87   in holothuroids, the number of such transcriptomic studies and the diversity of species

88   investigated remains limited.

89   The present study aimed to morpho-functionally describe the cœlomocytes of *H.*

90   *scabra*. Firstly, the different types of cœlomocytes were characterised using scanning

91   electron microscopy (SEM) and transmission electron microscopy (TEM) and a

92   comparison of the cell population was carried out between the HF and the PF.

93   Secondly, the immune response of cœlomocytes was studied 24 hours after an LPS

94   injection by investigating the change in the cœlomocyte population and identifying the

95   immune gene expression using *de novo* RNA-seq. Overall, our results provide a

96   general overview of the immune response in *H. scabra*, from the molecular to the

97   cellular level, and will contribute to a better understanding of immune mechanisms in

98   holothuroids.

99   ## 2. <u>Material and Methods</u>

100   ### 2.1. Specimen collection and handling

101   Specimens of *Holothuria scabra* Jaeger, 1833 were collected in the sea pens of the

102   Indian Ocean Trepang (IOT) company in Belaza (23°29'13.2"S; 43°45'32.4"E) and

103   Andrevo, Madagascar (23°01'15.6"S; 43°31'22.8"E) in November (**Fig. 1**). They were

104   harvested by hand and by snorkelling at night time (between 2 and 3 m deep at high

105   tide, seawater temperature = 26.5°C) to induce as little stress as possible. On the boat,

106   they were directly placed in seawater tanks before being brought back to the *Institut d'*

107   *Halieutique et des Sciences Marines* (IH.SM) of the Toliara University where they were

108   kept in tanks of 1 µm-filtered seawater (pH = 8.5; salinity = 34 psu; and temperature =

109   26°C). All used specimens were initially born within hatcheries of the IOT company,

110   requesting no specific permissions for this study on endangered organisms.

5
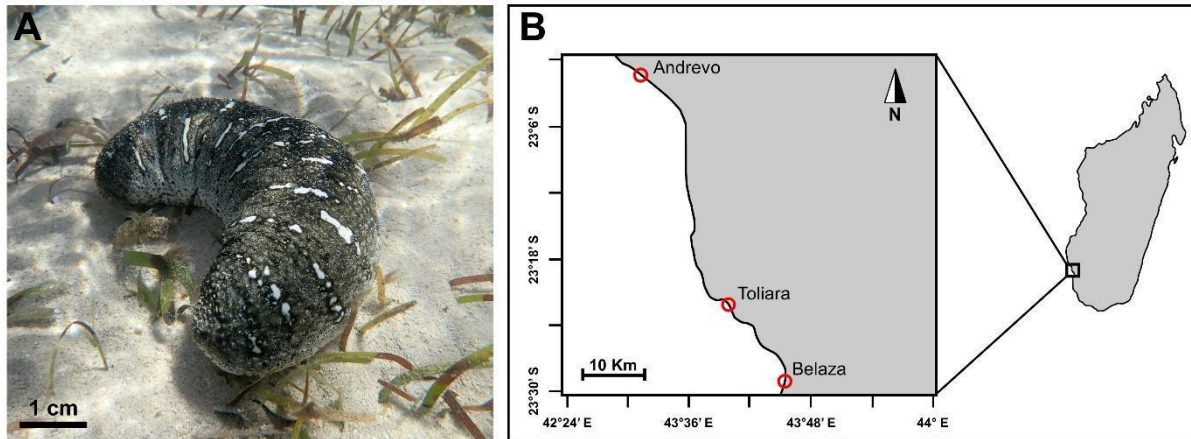
Fig. 1. Collection of *H. scabra* in Madagascar. A. Picture of an *in-situ* specimen (picture from GC). B. Map illustrating the different collection sites in the sea pens of the IOT company (Andrevo and Belaza) and the place where specimens were preserved for the study (*Institut Halieutique et des Sciences Marines* in Toliara).

2.2. Cœlomocyte harvesting and processing

Cœlomocytes were harvested from two body fluids: the perivisceral fluid (PF) and hydrovascular fluid (HF). Initially, a longitudinal incision was carried out on the *bivium*, from the posterior to anterior part, to open the perivisceral cavity and collect the PF. Then, the Polian vesicle was isolated and poured to harvest the HF. Depending on the following process, cœlomocytes were either directly observed under a microscope or mixed with an equivalent volume of artificial cœlomic fluid (aCF) (25 mM dithiothreitol; 10 mM $CaCl_2$; 50 mM MCl_2; 14 mM KCl; 398 mM NaCl; 1.7 mM $NaHCO_3$ and 25 mM Na_2SO_4; pH = 7.4) as per Smith et al. [13].

2.3. Cœlomocyte morphotype description

2.3.1. Light microscopy and morphotype abundance estimation

To establish the concentration and proportion of each cell type in a normal homeostasis state, the HF and PF of 9 individuals from two different aquaculture sites were collected (4 from Andrevo and 5 from Belaza; **Fig. 1B**). Then, 10 µL of each body fluid was loaded on a Neubauer hemacytometer and the 16 subdivisions of the slide, corresponding to a total volume of 0.1 mm^3, were photographed under a microscope

6

133 (CX41, Olympus). Cœlomocyte morphotypes were identified based on previous

134 cœlomocyte descriptions in other sea cucumber species [4,8] and were counted

135 manually using the ImageJ software (V1.40g). Cell concentrations were converted in

136 million cells per ml and the results were formulated as mean ± standard deviation (SD).

137 Proportions were calculated as the number of cells of the morphotype considered out

138 of the total number of coelomocytes (all morphotypes together) and converted into

139 percentages.   To reveal any relation in the concentration and proportion of

140 cœlomocytes between the two body fluids of the different individuals, a statistical

141 analysis was performed on Prism software (V5.03): firstly, a paired statistical test was

142 carried out to reveal potential differences (Wilcoxon matched pair signed rank test; α

143 = 5%); secondly, a correlation test was achieved to reveal a potential correlation

144 between the two fluids (Pearson correlation; α = 5%). Furthermore, a statistical test

145 was performed to highlight potential site-specific differences in coelomocyte

146 proportions and concentrations (between Andrevo: n = 4 and Belaza: n = 5; Mann

147 Whitney test; α = 5%).

148   2.3.2. Scanning Electron Microscopy (SEM)

149 The PF and the HF were immediately mixed with the aCF solution and centrifuged at

150 500 g and room temperature for 5 minutes. Pellets were then suspended in 1 ml of a

151 culture medium (500 mM NaCl; 5 mM $MgCl_2$; 1 mM EGTA and 20 mM of HEPES; pH

152 = 7.2) as per Smith et al. [13], and 150 µl were deposited on pre-cut histological slides

153 of 25 mm^2. The slides were incubated in a humid chamber for 30 minutes, following

154 the same protocol [13], so that cœlomocytes could adhere to the slides. After that,

155 cœlomocytes were fixed successively in a prefix solution (0.001% glutaraldehyde in

156 the culture medium; pH = 7.2) for 5 minutes and in a fixative solution for 1 hour (3%

157 glutaraldehyde, 0.1 M sodium cacodylate and 1.55% NaCl; pH = 7.4). Once fixed,

7

158   slides were rinsed in five successive baths of phosphate-buffered saline (PBS; 137

159   mM NaCl; 2.7 mM KCl; 10 mM Na_2HPO_4; 1.76 mM KH_2PO_4; pH = 7.4) and distilled

160   water. Then, cœlomocytes were dehydrated in seven successive ethanol baths of

161   increasing concentration (3 baths at 70% for 30 minutes, 1 night for 30 minutes; 2 baths

162   at 90% for 30 minutes and 1 bath at 100% for 1 hour) and chemically dried in six

163   successive baths of hexamethyldisilazane (HMDS) of increasing concentration in

164   ethanol (1 bath at 33%; 1 bath at 50%; 1 bath at 66% and 3 baths at 100%), the last

165   bath being let evaporated overnight under a fume hood. Once dried, slides were coated

166   with mixt of gold and palladium (40% and 60%, respectively; JFC-1100E metalliser,

167   Jeol) and observed and photographed with a scanning electron microscope (JSM-

168   7200F, Jeol).

169   2.3.3. Transmission Electron Microscopy (TEM)

170   PF and HF were immediately mixed to an equal volume of the aCF solution and

171   centrifuged at 900 g at room temperature for 2 minutes. The pellets were suspended

172   in the same cold fixative solution as for the SEM (see 2.3.2.) and stored at 4°C. After

173   three rinsing of 10 minutes with a cacodylate buffer (*i.e.* successive centrifugations and

174   pellet suspensions; 0.1 M sodium cacodylate and 1.55% NaCl; pH = 7.4), the pellets

175   were post-fixed in 1% osmium tetroxide in the same cacodylate buffer. Pellets were

176   once again rinsed three times for 10 minutes in the cacodylate buffer before a

177   dehydration step with 7 successive ethanol baths of increasing concentration (1 bath

178   at 25% for 10 minutes; 1 bath at 50% for 10 minutes; 1 bath at 70% for 20 minutes; 2

179   baths at 90% for 15 minutes; 2 baths at 100% for 30 minutes). Samples were then

180   embedded in Spurr resin. Finally, ultrathin sections (90 nm thick) were cut using an

181   ultramicrotome (Leica UCT) equipped with a diamond knife, collected on copper grids,

182   and contrasted with uranyl acetate for 45 minutes and lead citrate for 4 minutes and

8

183 30 seconds, successively. Samples were observed and photographed with a

184 transmission electron microscope (LEO 906E, Zeiss).

185 **2.4. Immune response**

186 2.4.1. Variation in cœlomocyte morphotype concentration

187 To identify modifications in cœlomocyte populations after the injection of

188 lipopolysaccharides (LPS) three conditions were considered: a LPS injection group (n

189 = 4), inoculated with 100 µL of sterile seawater containing 5 mg/ml of

190 lipopolysaccharide from *Escherichia coli* O111:B4 (L2630; Sigma-Aldrich); a control

191 injection group (n = 4), inoculated with 100 µL of sterile seawater and a no injection

192 group (n = 4), receiving no injection at all. The injections were carried out using a 1 ml

193 syringe and a 23g needle in the right anterior part. Specimens used for this

194 experimentation were all collected at the same location in Andrevo and were kept 24

195 hours in a tank before the experimentation. PF and HF were harvested 24 hours after

196 the injections to quantify the cœlomocytes on a hemacytometer and the concentration

197 of each cell type was calculated as explained above (see 2.3.1). Finally, a two-by-two

198 statistical test was performed in Prism software (V5.03) to reveal potential significant

199 differences between the three different conditions (Mann Whitney test; α = 5%).

200 2.4.2. Transcriptomic analysis of the immune response to LPS

201 *2.4.2.1. Immunostimulation and cœlomocyte processing*

202 Transcriptomic analysis was carried out on cœlomocytes from PF and two conditions

203 were compared for the final purpose of identifying the immune differentially expressed

204 genes (IDEGs): a LPS injection group as test condition (n = 3) and a control injection

205 group as a control condition (n = 3). All specimens came from the same sea pen in

206 Andrevo and were kept 24 hours in a tank before the experimentation. Coelomocytes

207 from the PF have been shown to have a wide range of immune gene expression

9

208 [11,12,14], and it is also easier to collect a large volume of the PF compared to HF,

209 hence the decision to focus the transcriptomic analysis on this body fluid. Injections

210 were carried out in the same way as for the study of variation in cœlomocyte

211 populations (see section 2.4.1.), 24 hours before harvesting the PF. Once isolated, the

212 PF was directly mixed with the same volume of the aCF to avoid the clotting of

213 cœlomocytes and the mixture was centrifuged at 500 g for 5 minutes at room

214 temperature. Pelleted cells were then suspended in RNAlater® (R0901; Sigma-

215 Aldrich) and stored at 4°C until their transfer to the Belgian laboratory (University of

216 Mons). There, the tubes were centrifuged again at 500 g at 4°C for 5 minutes to remove

217 the RNAlater® and the pellets were stored at -80°C until RNA extraction.

218   *2.4.2.2.   RNA extraction, cDNA library preparation and sequencing*

219 RNA extractions were performed using the RNeasy Mini kit (Qiagen) following the

220 manufacturer's instructions. The concentration and purity of the extracted RNA were

221 determined using a nanodrop spectrophotometer (Denovix DS11) and the RNA

222 integrity value (RIN) was assessed using the Agilent 2100 Bioanalyzer (Agilent RNA

223 6000 Nano kit). The preparation of cDNA libraries and the sequencing were performed

224 by the Beijing Genomics Institute (BGI, Hong Kong). Briefly, cDNA libraries were built

225 as follows: mRNAs were isolated from total RNA using the oligo(dT) method; purified

226 mRNAs were fragmented, and reverse transcribed into the first strand of cDNA, before

227 the synthesis of the second strand of cDNA; double-stranded cDNA fragments were

228 end-repaired, 3'-adenylated and connected with Illumina adapters; cDNA fragments of

229 appropriate size were selected and enriched by PCR. After validation using the Agilent

230 2100 Bioanalyzer, the library was sequenced using the Illumina HiSeq™ 2000

231 sequencer and the resulting sequence data (raw reads) was retrieved in FASTQ

232 format. Regarding data availability, raw reads are currently under submission as NCBI

233 sequence read archive and the assembly will be shared under request.

234   *2.4.2.3. Raw data filtering and* De novo *assembly*

235 Before the assembly, raw read data were filtered to remove adapter-polluted reads,

236 reads containing more than 5% of unknown bases and low-quality reads (*i.e.* reads

237 comprising more than 20% of bases with a quality value of less than 10). The

238 transcriptome was assembled *de novo* using the Trinity software (V2.0.6). The

239 resulting transcripts were then clustered using Tgicl software (V2.0.6) to eliminate

240 redundancy and obtain the final sequences called unigenes. The unigenes can either

241 form clusters comprising several unigenes with more than 70% overlapping or

242 singletons (*i.e.* single unigenes). As the sequence length is a criterion of the assembly

243 quality, the size distribution of unigenes was represented.

244   *2.4.2.4. Transcriptome completeness and functional annotation*

245 To assess the completeness, BUSCO statistic was assessed for each individual

246 transcriptome and the merged results using the tool BUSCO in the Galaxy server

247 (https://usegalaxy.eu; V5.4.6). The BUSCO metrics attempt to provide a quantitative

248 assessment of the completeness of genomics data by classifying orthologs into the

249 four following categories: complete and single-copy, complete and duplicated,

250 fragmented, or missing BUSCOs [15].

251 To have a first indication of the unigene function, the sequence of each unigene was

252 aligned   against   several   protein   databases   including   NCBI   NT

253 (http://www.ncbi.nlm.nih.gov.), NCBI NR (http://www.ncbi.nlm.nih.gov.), GO – Gene

254 Ontology (http://www.geneontology.org), KOG – EuKaryotic Orthologous Groups

255 (http://.ncbi.nih.gov/pub/COG/KOG), KEGG – Kyoto Encyclopedia of Genes and

11

256   Genomes   (http://www.genome.jp/kegg),   SwissProt

257   (http://www.ebi.ac.uk/pub/databases/swissprot)   and   InterPro   (

258   http://www.ebi.ac.uk/interpro) using Blast (V2.2.23), Diamond (V0.8.31), Blast2GO

259   (V2.5.0) and InterProScan5 (V5.11-51.0). The annotation of unigenes provides an E-

260   value that quantifies the degree of annotation reliability: only annotations with an E-

261   value < 10^{-5} were considered. Overall, the NR annotation was preferred, except for

262   some unigenes for which the SwissProt annotation resulted in a gene having a specific

263   function in immunity that was not revealed by NR annotation (see section 2.4.2.7).

264   Moreover, the distribution of species among the Nr annotations was assessed to

265   highlight similarities with existing genomic data.

266   *2.4.2.5.   Gene expression level and identification of the differentially*

267   *expressed genes*

268   The expression level of each unigene was calculated following the "Fragments per

269   kilobase of transcripts, per million mapped reads" – FPKM method. FPKM is an

270   informative expression value that integrates the influence of the sequence length as

271   well as the sequencing level but does not directly inform about differential expression.

272   The differentially expressed genes (DEGs) were identified using the DESeq2 package.

273   The result consists of a fold change value which corresponds, for a given unigene, to

274   the ratio of the mean expression level between the test and the control conditions. The

275   fold change values (FC) were formulated as $\log_2$ for easier readability. In addition to

276   the FC, DESeq2 performed a Wald statistical test to check the significance of the

277   differential expression. The generated p-value is adjusted following the Benjamini–

278   Hochberg procedure and called the False Discovery Rate (FDR). Only the unigenes

279   having a $|\log_2(FC)$ value$| \geq 1$ and an FDR $\leq 5\%$ were considered as significantly

280   differentially expressed.

12

281 To represent the differential expression between the two conditions, the DEG FPKM

282 values were loaded in MetaboAnalyst (V5.0). After a $\log_{10}$ transformation and

283 autoscaling (mean-centred and divided by the SD of each DEG), a heatmap of DEGs

284 as well as a correlation matrix of individuals was constructed to represent the

285 differential expression and the individual heterogeneity, respectively.

286   *2.4.2.6.   Functional classification and enrichment analysis of GO terms and*

287   *KEGG pathways*

288 The GO and KEGG databases are useful bioinformatic resources which provide a

289 standardised classification of genes and proteins according to their ontology or

290 biological pathways, respectively. These databases were used to provide a general

291 functional description of the DEGs via enrichment analyses. Furthermore, KEGG

292 pathway enrichment was used to give the ten most enriched pathways, all categories

293 included, as well as the ten most enriched pathways among the KEGG organismal

294 system "immune system".

295   *2.4.2.7.   Identification of immune DEGs*

296 The immune DEGs (IDEGs) were identified based on their functional annotations.

297 Primarily, the KEGG pathway enrichment was used to provide the list of DEGs that

298 correspond to "immune systems" among the different organismal system pathways.

299 Secondly, a "keyword search" was performed among the DEG annotation list to find

300 genes of interest that were selected from different immune gene atlas in echinoderms

301 [4,16,17]. The results of these two searches were combined and only the most relevant

302 genes to the literature are presented in the results (see 3.2.2.5). This list was

303 represented as a heatmap: the gene expression was transformed as in 2.4.2.5. and

304 these values were extracted to build the final figure in Excel. IDEGs were classified

13

305 according to their presumed function to facilitate the readability and therefore, no
306 clustering was performed on this heatmap.

3. <u>Results and Discussion</u>

3.1. Cœlomocyte diversity

3.1.1. Morphological description of cœlomocyte types

310 Based on morphological characteristics, ten coelomocyte morphotypes were

311 distinguished, including five main morphotypes that were distinguishable by light

312 microscopy and five sub-types that were described based on their ultrastructure. The

313 five main morphotypes include phagocytes, small round cells (SMCs), spherulocytes,

314 fusiform cells and crystal cells.

315 Phagocytes were recognised by their numerous pseudopodia and their strong

316 adhesion to the slide (**Fig. 2A**). They were the largest cœlomocyte type with a diameter

317 measuring between 15 and 40 µm when considering pseudopodia, for a cell body

318 ranging from 4 to 10 µm (*i.e.* without pseudopodia). Phagocytes are traditionally

319 classified into two subtypes based on the shape of their pseudopods: filipodial

320 phagocytes bearing long and thin pseudopods called filipodia and petaloid phagocytes

321 bearing veil-like pseudopods called lamellipodia [18]. Although the two subtypes were

322 observed (**Fig. 2B** and **2C**, respectively), most phagocytes appeared to be an

323 intermediate between the two subtypes (*i.e.* they possessed both lamellipodia and

324 filipodia; **Fig. 2A**), and this is why no distinction has been made in the cell count. This

325 observation supports the hypothesis that these two types are two different stages

326 capable of transforming from one to the other, rather than distinct functional cell types.

327 Concerning their ultrastructure, only filopodial phagocytes were recognisable based on

14

328   their filipodia; they showed a large heterochromatic nucleus with peripheral

329   mitochondria and several lysosomes (**Fig. 3A**).

330   The small round cells (SRCs) measured between 4 and 6 µm (**Fig. 2D**), and their

331   ultrastructure consisted of a large nucleus occupying most of the cellular volume with

332   a dense cytosol containing many mitochondria (**Fig. 3B**). The same cell type was

333   observed in other species of holothuroids and referred to as either progenitor cells [6]

334   or lymphoid cells [19]. The name "progenitor cells" was given because their

335   undifferentiated appearance suggests they could be stem cells, giving rise to the other

336   types of cœlomocytes, while the name "lymphoid cells" was attributed according to a

337   resemblance to vertebrate lymphocytes. However, to date, the functions associated

338   with these cells remain to be demonstrated, and this is why we have preferred a non-

339   speculative name based only on their morphology.

340   Spherulocytes were identified through their numerous secretory granules (**Fig. 2E**).

341   Their diameter was highly variable, ranging from 5 to 20 µm. Based on their

342   ultrastructure, we were able to distinguish four subtypes: type I spherulocytes were the

343   smallest in diameter (5 - 9 µm) and showed homogeneous, electron-dense secretory

344   granules measuring between 0.5 and 1 µm (**Fig. 3C**); type II spherulocytes were the

345   largest (11 - 20 µm) and also had the biggest secretory granules (3 - 4.5 µm), showing

346   an electron-dense inner part and a loose outer part (**Fig. 3D**); type III spherulocytes

347   had an intermediate diameter (9 - 10 µm) and their secretory granules, measuring

348   between 1.2 and 1.5 µm, were filled of a not electron-dense fibrous material (**Fig. 3E**);

349   type IV spherulocytes were between 10 and 14 µm in diameter and had the highest

350   number of granules (> 80) but also the smallest (0.3 - 1 µm) (**Fig. 3F**), which were

351   electron dense. The nuclei were similar between the four sub-types; they were

352   irregularly shaped and measured between 1 and 4 µm. In terms of proportion, the two

15

353   first types were predominant while the two last were less represented on the thin

354   sections. The first three cell types seem to correspond to those observed in TEM in *H.*

355   *polii*, *A. japonicus* and *C. japonica* with a few size differences [6,20]. Furthermore,

356   Queiroz et al. [21] recently showed that it was possible to distinguish different types of

357   spherulocytes *sensus lato* according to the diameter of their cytoplasm and their

358   secretory granules in three species of the genus *Holothuria*. According to their

359   classification, type II spherulocytes would correspond to morula cells; type III

360   spherulocytes to acidophilic cells and type IV spherulocytes to spherulocytes *sensus*

361   *stricto,* but no cell type seems to correspond to type I spherocytes. Several studies

362   suggest that the different subtypes of spherulocytes are rather different stages of

363   maturation than true functional cell types [6,20]. For example, Eliseikina and

364   Magarlamov [6] also described "young morula cells" which are relatively small

365   spherulocytes containing many granules. This type of spherocyte is thought to be the

366   primitive stage and is more likely to correspond to type I or type IV spherulocytes based

367   on their size, appearance, and number of secretory granules. Therefore, this

368   continuum in maturation stages could explain the absence of certain subtypes across

369   the different studies, which could vary according to the homeostasis status of the

370   individuals, or the techniques employed to distinguish the different subtypes.

371   Fusiform cells were identified by their characteristics two opposite pseudopodia (**Fig.**

372   **2F**). In some of them, it was possible to distinguish a transition zone between

373   cytoplasmic projections of the cellular body and the pseudopodia, which was marked

374   by a slight swelling (**Fig. 2F**). In terms of size, their cellular body measured between 3

375   and 5 µm whereas their total length could exceed 30 µm considering their

376   pseudopodia.

16

377 Crystal cells were recognised based on their prismatic shape formed by their crystalline

378 inclusion. Indeed, these crystalline inclusions can take different shapes, thus varying

379 the shape of the cell itself; here, some were more rectangular while others were more

380 extended as in **Fig. 2G**. Their size generally varied from 7 to 14 µm but the most

381 elongated ones could reach 25 µm in length.

382 These two last cell types could not be observed in TEM, probably because of the

383 difficulty of finding poorly represented cell types in TEM preparations. In SEM,

384 however, the fusiform cells were easily identifiable while the crystal cells were rarely

385 observed. We identified the one in **Fig. 2G** according to its close resemblance in both

386 size and morphology to the crystal cells observed under light microscopy. However,

387 whether it is a crystal cell remains speculative and therefore we preferred to report this

388 cell as an "assumed crystal cell".

389 In addition to cœlomocytes recognisable under light microscopy, a cell type was only

390 observed in the TEM preparations and was identified based on its particular

391 ultrastructure; it showed a high number of small vacuoles measuring between 0.2 and

392 1 µm in diameter, some of which contained residual bodies (**Fig. 3G** and **3H**). These

393 characteristics of vacuolated cells were previously described in the species *A.*

394 *japonicus* and *C. japonica* [6]. In these species, vacuolated cells were reported to

395 achieve amoeboid movement and to increase in concentration when foreign particles

396 are injected into the body wall (unpublished data from [6]). Based on their morphology,

397 it was suggested they could participate in the storage and regulation of calcium ions

398 [6]. Although we do not exclude this hypothesis, the presence of residual bodies inside

399 some vacuoles, which is reminiscent of phagosome-like structures, plus the fact that

400 their abundance seems to correlate with physiological stress, rather suggest that they

401 would be dehiscent phagocytes that have already phagocytosed foreign bodies.

17

402 Furthermore, this is consistent with the fact that individuals dedicated to the
403 cœlomocyte morphological description in this study came directly from the natural
404 environment and could be exposed to numerous stressors just before the experiment.
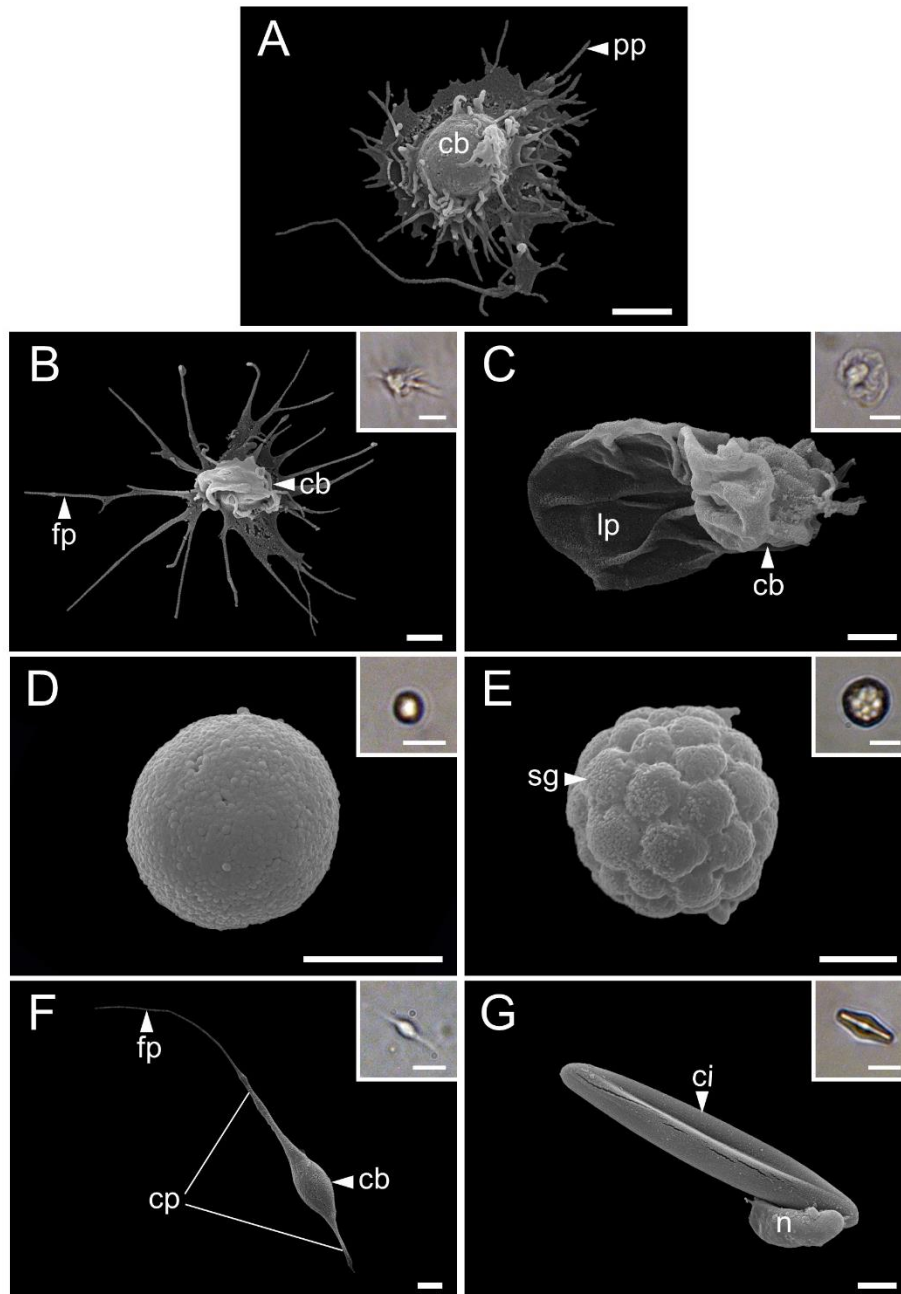
405

406 **Fig. 2.** Cœlomocyte morphotypes in the body fluids of *H. scabra* (light and scanning
407 electron microscopy views). A. Intermediate phagocyte. B. Filiform phagocyte. C.
408 Petaloid phagocyte. D. Small round cell (SRC). E. Spherulocyte. F. Fusiform cell. G.
409 Assumed crystal cell. Legend: cb – cellular body; cp – cytoplasmic projection; ci –
410 crystalline inclusion; fp – filipodia; lp – lamellipodia; pp – pseudopod; n – nucleus; sg –

18

secretion granule. The scale bars represent 2 μm in large images (SEM) and 10 μm in small images (light microscopy).
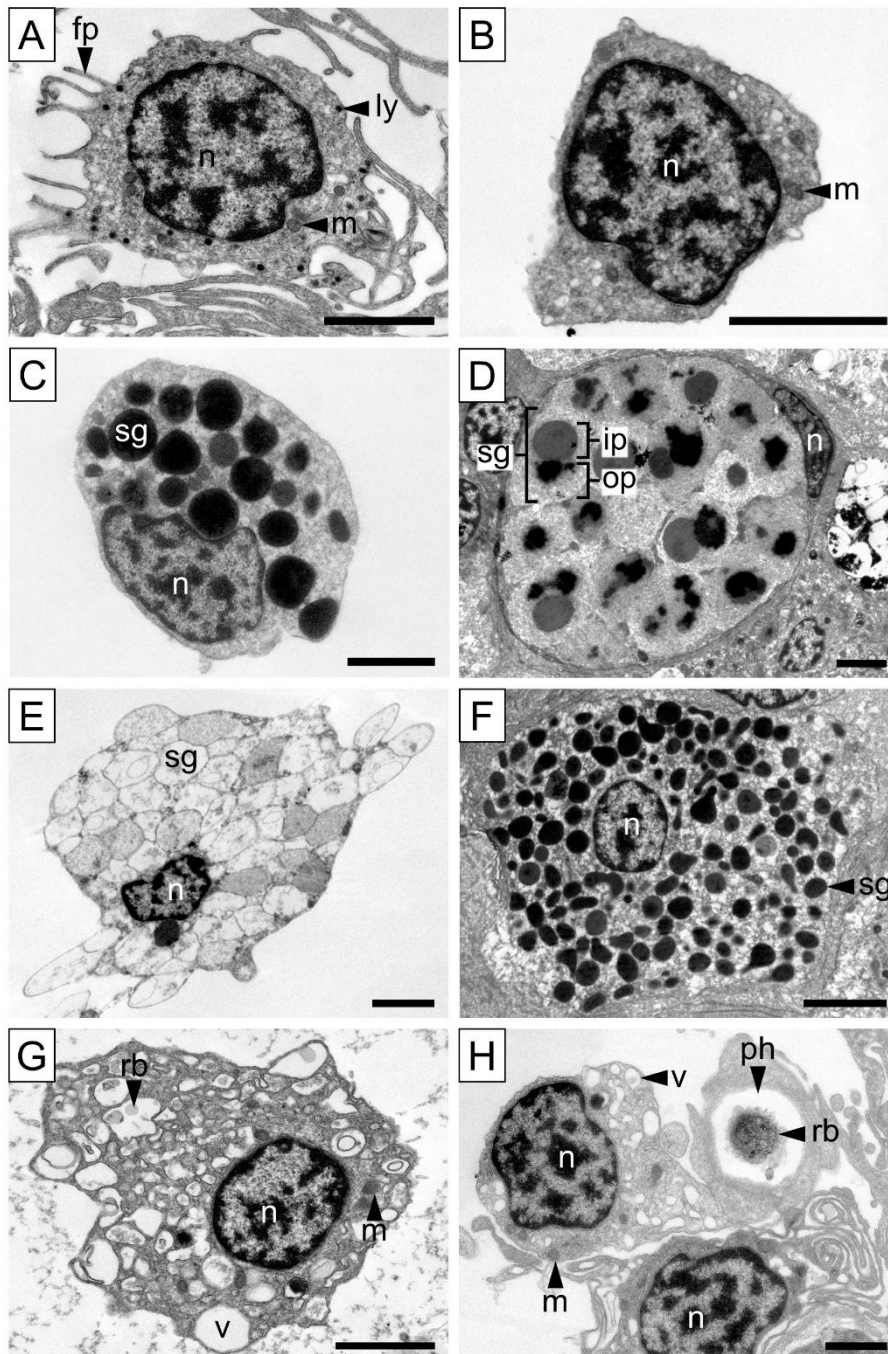
Fig. 3. Ultrastructure of cœlomocyte morphotypes in *H. scabra*. A. Filiform phagocyte. B. Small round cell (SRC). C. Type I spherulocyte. D. Type II spherulocyte. E. Type III spherulocyte. F. Type IV spherulocyte. G. Vacuolated cell. H. Vacuolated cell (up-right) and filiform phagocyte (down-left) with a phagosome-like structure containing a residual body. Legend: fp – filipodia. ip – inner part of the granule; ly – lysosome; m – mitochondria; n – nucleus; op – outer part of the granule; ph – phagosome-like structure; pp – pseudopod; rb – residual body; sg – secretory granule; v – vacuole. The scale bars represent 2 μm.

19

422   3.1.2. Cœlomocyte concentration and proportion in the body fluids of *H. scabra*

423   The total cœlomocyte concentration was $3.5 \pm 1.8 \ 10^6$ cells ml^{-1} in the HF and $1.7 \pm$

424   $1.2 \ 10^6 \ ml^{-1}$ in the PF of *H. scabra* (n = 9). **Table 1** summarises the concentration and

425   proportion values for each of the 5 cell types that were identified under light microscopy

426   in the HF and PF. In both fluids, phagocytes were the dominant type with a proportion

427   of $71.5 \pm 17.5\%$ and $60.8 \pm 24.6\%$, respectively. These numbers are consistent with

428   the previous report of Prompoon et al. [9] who reported a proportion of 60.2% in the

429   PF of *H. scabra*, and it also corresponds to the proportion reported in other holothuroid

430   species [5,20,21]. The second most abundant cell type varies across holothuroid

431   species: for example, it is spherulocytes in *Holothuria polii* while it is progenitor cells

432   (here referred to as small round cells (SRCs), see 3.1.1) in the species *Holothuria*

433   *grisea* ([20] and [21], respectively). In *H. scabra*, we found that SRCs were more

434   abundant than spherulocytes, with a proportion of about 25% in both fluids. Again, this

435   proportion reflects the previous study of cœlomocytes in *H. scabra* that reported a

436   proportion of 25.2% in the PF [9]. Spherulocytes accounted for only $3.4 \pm 2.3\%$ and

437   $7.0 \pm 8.5\%$ in HF and PF, respectively. These proportions are weaker compared to

438   other species of the genus *Holothuria* [20,21], and it is also lower than the 12.8%

439   previously reported in the PF of *H. scabra* [9]. The last two cell types, fusiform cells,

440   and crystal cells were observed in both fluids but not necessarily in all individuals; out

441   of the nine investigated individuals, fusiform cells were observed in the HF of 7

442   individuals (77%) and the PF of 4 individuals (44%) whereas crystal cells were

443   observed in the HF of 3 individuals (33%) and the PF of all individuals. The fact that

444   we did not observe them in all individuals does not necessarily mean that they were

445   not always present in the body fluids since both cell types were reported at low

446   concentrations [8,21]. Their absence in some individuals was also reported in other

20

species [18], and it was even suggested that fusiform cells are restricted to the PF in the species *Cucumaria frondosa* [5]. These two cell types were not reported by Prompoon et al. [9] which could be attributed to the lectin-based flow cytometry approach they employed, making it challenging to identify less abundant cell types accurately. A last cell type could be observed in the body fluids of 3 individuals (30%) it was a flagellated cell type that would be traditionally attributed to vibratile cells (*e.g.* [4,18]). However, Caulier et al. (EDS) [22] have recently shown that this cell type corresponds to contaminating spermatozoa in holothuroids, which are difficult to avoid when collecting body fluids in males and this is why we have decided not to include this non-immune cell type in our study.

Table 1. Concentration and proportion of each cœlomocyte type in the hydrovascular fluid (HF) and perivisceral fluid (PF) of *H. scabra*. Results are formulated as mean ± SD (minimum value – maximum value) (n = 9). The p-values show significant differences between the two body fluids (Wilcoxon paired signed rank test; p-values ≤ 5% are in bold).

Cell types	Concentration (cells ml^{-1})			Proportion (%)		
	HF	PF	p-value (W)	HF	PF	p-value (W)
Phagocytes	2.54 ± 1.62 (0.42 – 5.85) 10^6	9.22 ± 4.47 (4.4 – 14.5) 10^5	**2.7 10^{-2} (37)**	71.5 ± 17.5 (41.4 – 93.8)	60.8 ± 24.6 (25.1 – 82.2)	0.2 (23)
Small round cells (SRCs)	8.2 ± 9.61 (1.40 – 30.5) 10^5	6.52 ± 10.11 (0.3 – 32.3) 10^5	0.26 (17)	23 ± 18.7 (4.1 – 56.6)	28.4 ± 23.4 (4.6 - 68)	0.73 (-7)
Spherulocytes	1.01 ± 0.87 (0.3 – 3.2) 10^5	1.09 ± 1.52 (0.1 – 5) 10^5	0.2 (16)	3.4 ± 2.3 (1.1 – 7.3)	7.0 ± 8.5 (0.6 – 28.6)	0.64 (8)
Fusiform cells	4.44 ± 4.27 (0 – 11.1) 10^4	2 ± 3.42 (0 – 10) 10^4	0.86 (4)	1.6 ± 1.8 (0 – 5.3)	1.4 ± 2.5 (0 – 5.7)	0.19 (-23)
Crystal cells	4.44 ± 7.26 (0 – 20) 10^3	4.7 ± 3 (1 – 8) 10^4	**1.33 10^{-2} (-36)**	0.4 ± 1 (0 – 3.1)	2.8 ± 1.4 (1.1 – 4.9)	**1.76 10^{-2} (-41)**
Total	3.51 ± 1.81 (0.64 – 6.24) 10^6	1.75 ± 1.21 (0.65 – 4.75) 10^6	7.42 10^{-2} (31)	100	100	100

462

463   3.1.3. Relation between the cœlomocytes of the HF and the PF

464   Surprisingly, only a few studies have examined cœlomocytes from the HF (*e.g.* [5,22]),

465   and even fewer have compared cœlomocyte abundance and diversity between the two

466   body fluids (*e.g.* [19]). Here, we compared the concentration and proportion between

467   these two fluids and tried to correlate these values to see if there is any influence of

468   individuality on these metrics. Overall, the statistical test reveals no significant

469   difference in the concentration and proportion between the HF and the PF, except for

470   phagocytes in concentration and crystal cells both in concentration and proportion

471   (**Table 1**). The fact that phagocytes differ significantly in concentration but not in

472   proportion is likely because, as the most represented cell type, they follow the variation

473   in the overall total number of coelomocytes, which is also close to the significance in

474   terms of concentration ($p = 7.42 \times 10^{-2}$; $W = 31$). Regarding crystal cells, their higher

475   concentration and proportion in the PF suggest that this cell type is more restricted to

476   this body fluid.

477   The correlation tests between the two body fluids were for most cell types weak ($r < 6$)

478   and not significant ($p > 5\%$; see **Table 2**). Most of the concentrations were negatively

479   correlated between the two fluids. These negative correlations could reflect a transfer

480   from one compartment to the other. In contrast to other cell types, SRCs had a positive

481   correlation both in concentration and proportion at $r = 0.41$ and $r = 0.68$, respectively,

482   and a significant correlation only for the proportion ($p = 4 \times 10^{-2}$). These cells were

483   previously described as stem cells [6], and the coelomic epithelium and the Polian

484   vesicle, which respectively enclosed the PF and the HF, were reported to be potential

485   haematopoietic tissues [23]. Therefore, the production of SRCs in the PF and HF would

486   be stimulated by the same physiological pathways and would thus be concomitant,

487   explaining these positive correlations. However, this would not be the case for the

22

488 differentiated cell types that would rather migrate toward the body area where the

489 infection and/or the injury occur(s).

Table 2. Correlation of the concentration and the proportion for each cœlomocyte type between the hydrovascular fluid and the perivisceral fluid (r = Pearson correlation coefficient; r^2 = determination coefficient; p-values show significant correlations; p-values ≤ 5% are in bold).

	Concentration			Proportion		
Cell types	r	r^2	p-value	r	r^2	p-value
Phagocytes	-0.59	0.34	0.097	0.56	0.31	0.12
Small round cells (SRCs)	0.41	0.16	0.28	0.68	0.47	**0.04**
Spherulocytes	-0.23	0.05	0.55	-0.06	0.00	0.87
Fusiform cells	-0.15	0.02	0.693	0.14	0.02	0.73
Crystal cells	-0.50	0.25	0.173	-0.32	0.10	0.40
Total	-0.26	0.07	0.508	1.00	1.00	0.00

496 Overall, we were not able to reveal any clear relation between the HF and the PF,

497 suggesting that the influence of individuality on cœlomocyte concentration and

498 proportion is weak or at least more complex than expected. This conclusion

499 corroborates the previous study of Li et al. [19] that could find much the same cell types

500 in both fluids but failed to demonstrate a clear relationship in the cell type concentration

501 or proportion between the two fluids.

502   3.1.4. Influence of the aquaculture sites on coelomocyte concentration and

503   proportion

504 The comparison between the two aquaculture sites can be viewed in **Supplementary**

505 **Material 1**. Although some differences are visible in the concentration and proportion

506 of cœlomocyte types, in particular the concentration of spherocytes in the PF, which is

507 significantly higher in the Belaza site ($p = 2 \times 10^{-2}$; U = 0), it can be noted that the order

508 of morphotypes in concentration and proportion is the same between the two

509 aquaculture sites, thus highlighting a typical coelomocytes profile of normal

510 homeostasis condition.

511   3.1.5. Cœlomocyte aggregates

512 The examination of the body fluids also reveals the presence of numerous cellular

513 aggregates that were mainly composed of phagocytes, spherulocytes and SRCs (**Fig.**

514 **4A-D**). These aggregates have been termed "early aggregates" because their size and

515 number seemed to correlate with the time post-body fluid collection. Three types of

516 early aggregates could be distinguished according to their size and appearance –

517 probably corresponding to successive stages of maturation: small aggregates,

518 measuring between 20 and 100 µm, were of limited cell number and were completely

519 colourless (**Fig. 4A**); intermediate aggregates, measuring about 100 µm, had some

520 brownish spots and were denser (**Fig. 4B**); large aggregates, measuring between 100

521 and 200 µm, were fully pigmented and their high density made it difficult to distinguish

522 cells constituting them (**Fig. 4C**). Aggregation of cœlomocytes is usually observed

523 during the body fluid collection and the use of an anticoagulant solution is often

524 necessary to avoid this phenomenon [13]. This aggregation is related to encapsulation,

525 an important cellular mechanism in innate immunity that consists of entrapping a

526 foreign body in a cellular aggregate [24]. This mechanism is well described in

527 arthropods and involves a melanisation phenomenon that implicates the deposition of

528 melanin within the aggregate to isolate the foreign body and also involves the

529 production of reactive oxygen species to degrade this body [24]. Thus, the colour

530 change that is observed between the three early aggregate stages could be attributed

531 to this melanisation process.

24

532 In addition to the early aggregates, large brown aggregates were observed on the inner

533 wall of the Polian vesicle (**Fig. 4E**). These aggregates were much larger than those

534 found in cell suspension with a diameter ranging from 150 to 1000 µm. They appeared

535 to be mainly composed of small cells similar in size to SRCs, although a few

536 spherulocytes could be observed in some of them (**Fig. 4F**). In contrast to the early

537 aggregates, these brown aggregates seemed to pre-exist in the collection of the body

538 fluids and were only observed in the hydrovascular compartment. Such coloured

539 aggregates have been observed in several species of echinoderms and have

540 historically been referred to as brown bodies. Recently, Jobson et al. [25] showed that

541 the colour of these aggregates varied according to the class of echinoderm considered,

542 thus matching the phylogeny of extant echinoderms. Furthermore, Caulier et al. [5]

543 suggested that these aggregates could change in colour depending on the body

544 compartment in which they were found in the holothuroid species *C. frondosa*, ranging

545 from red in the HF to brown in the PF. The red colour of these aggregates would be

546 due to the presence of hemocytes, a type of cœlomocyte containing haemoglobin,

547 rather than a melanisation process. The presence of these cells was recently reported

548 in the HF of several species of the genus *Holothuria*, including *H. scabra* [22]. However,

549 in *H. scabra* the colour of the cell was brown rather than red; it was suggested that

550 under certain conditions, for example under different oxygen concentrations, the colour

551 of hemocytes may vary and become less intense. A lack of colour could thus explain

552 why we failed to identify them in the cell suspension of the HF. Another reason could

553 be that, in the immunoquiescent state, these cells remain marginalised, *i.e.* attached

554 to the membrane of the adjacent tissues [5]. Hence, a large proportion of hemocytes

555 could have remained attached to the membrane of the Polian vesicle during HF

556 harvesting.

557 Overall, while the early aggregates would correspond to the initial stages of
558 encapsulation, brown aggregates would rather correspond to the result of this process,
559 or at least to a deposition of particular cells that pre-exists the body fluid collection.
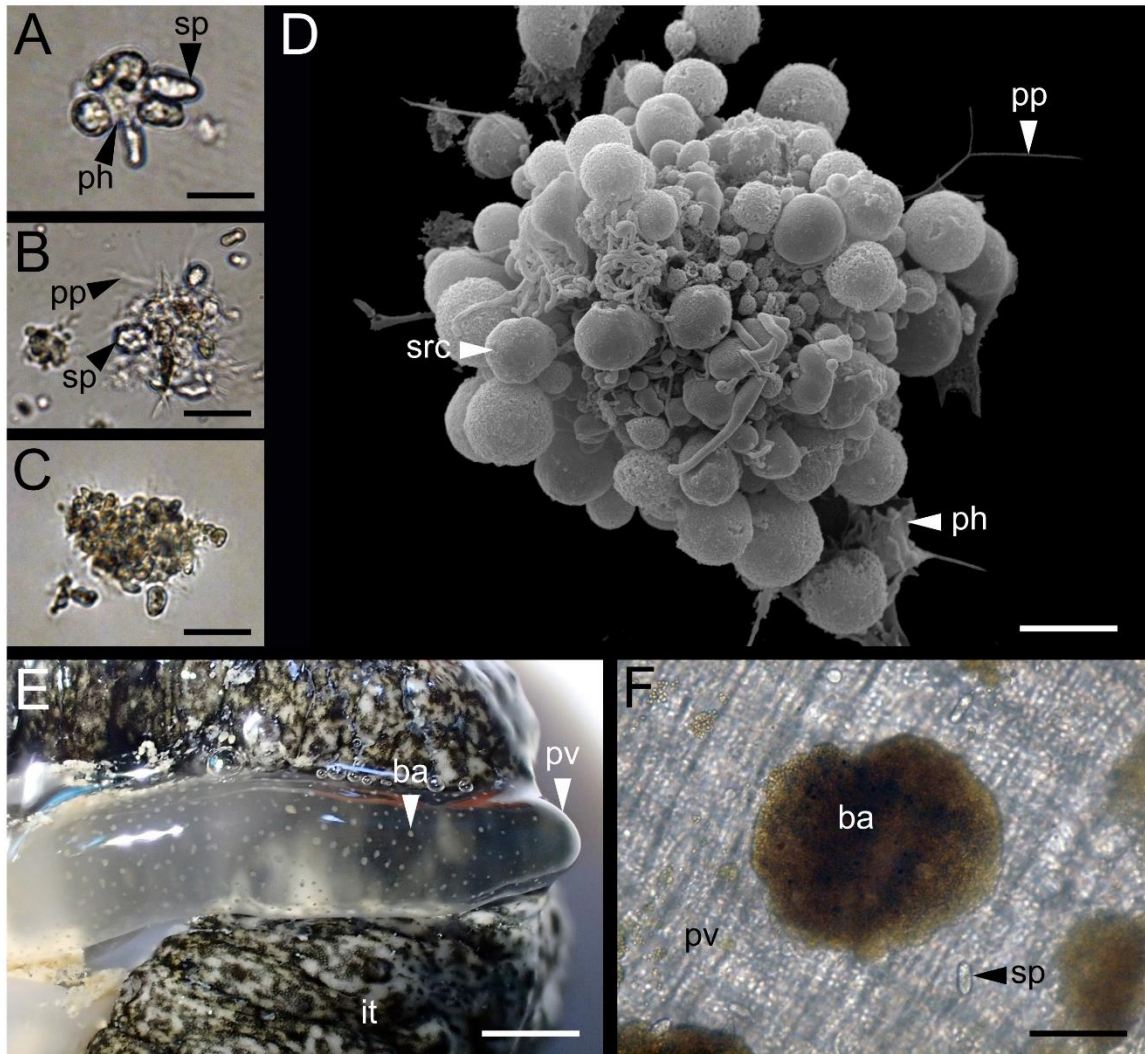
560

561 **Fig. 4.** Cœlomocyte aggregates in *H. scabra*. A. Small uncoloured aggregate. B.
562 Intermediate aggregate harbouring pigmented spots. C. Large aggregate fully
563 pigmented. D. SEM picture of a cœlomocytes aggregate. E. Polian vesicle showing
564 coloured aggregates. F. Optical view of the coloured aggregates on the internal wall of
565 the Polian vesicle. Legend: ba – brown aggregate; it – integument; ph – phagocyte; pp
566 – pseudopod; pv – Polian vesicle; sp – spherulocyte; src – small round cell. The scale
567 bars represent 20 µm in A; 30 µm in B; 40 µm in C; 5 µm in D; 4 mm in E; and 60 µm
568 in F.

26

569 **3.2. Immune response of cœlomocytes**

570　3.2.1. Modification in cœlomocyte concentration and proportion

571　The result of cell variation in response to injections varied among the different

572　cœlomocyte types, both in concentration and proportion (**Fig. 5**). First regarding the

573　concentration, comparisons between the different conditions revealed a significant

574　increase of SRCs in the PF (p = 2.9 10^{-2}; U = 0), and a significant decrease of

575　spherulocytes in the HF (p = 4 10^{-2}; U = 0.5), both between the no injection group and

576　the LPS injection group. These significant results were observed neither between the

577　control injection and the LPS injection groups nor between the no injection and the

578　control injection groups. This can be partly explained by the high standard deviations,

579　particularly within the control injection group (**Fig. 5**).

580　In terms of proportions, only spherulocytes showed a significant difference, with a

581　decrease in the HF of the LPS injection group compared to the no injection group (p =

582　2.9 10^{-2}; U = 0.5). This decrease was not observed within the PF for the LPS injection

583　group with a slight increase compared to the no injection group. Besides, although not

584　significant, a similar tendency was observed in the two body fluids and was also the

585　same between the two injection groups, namely, a decrease in the phagocyte

586　proportion concomitant with an increase in the SRC proportion (**Fig. 5**).

587　SRCs are assumed to be progenitor cells that can differentiate into other types of

588　cœlomocytes [6]. Their production could therefore be stimulated to counteract the loss

589　of effective immune cells such as phagocytes as suggested by the tendency of

590　phagocytes to decrease in proportion. Regarding spherulocytes, they play important

591　functions in the immune response, including in the production of various humoral

592　factors, encapsulation and wound healing [4]. Their weaker concentration and

593　proportion in the LPS injection group could be explained by their implication in the

27

594   immune response that could lead to an apoptotic-like process after degranulation or

595   participation in the cell aggregate formation. This decrease is nevertheless not

596   observed in the PF with an increase in the LPS injection compared to the no injection

597   group both in terms of concentration and proportion. This opposite dynamic could

598   suggest the recruitment of spherulocytes in the PF, which is more prone to be the place

599   of infections as it is confined in the general cavity just below the integument physical

600   barrier. Furthermore, a higher SRC proportion compared to phagocytes was not

601   observed in control individuals, regardless of the aquaculture site considered (*i.e.* no

602   injection individuals; see section 3.1.4.). This supports the occurrence of a

603   coelomocyte profile specific to "immunological stress" in *H. sabra*. The full result of the

604   statistical analyses can be consulted in **Supplementary Material 2**.

605   Overall, these results reflect the high inter-individual variability in cœlomocyte

606   populations suggesting complex and rapid regulation mechanisms in the production

607   and activation of cœlomocytes. It also indicates that cœlomocyte counting is not

608   necessarily the best indicator for stress evaluation in *H. scabra*, as it was reported in

609   other echinoderm species (*e.g. Paracentrotus lividus* [26]). At the very least, as it has

610   been shown that holothuroids can rapidly modulate their water content in case of

611   environmental stresses [27], we advise using the proportion as an indicator rather than

612   the concentration, which depends directly on the fluid volume in the organism.

28

613
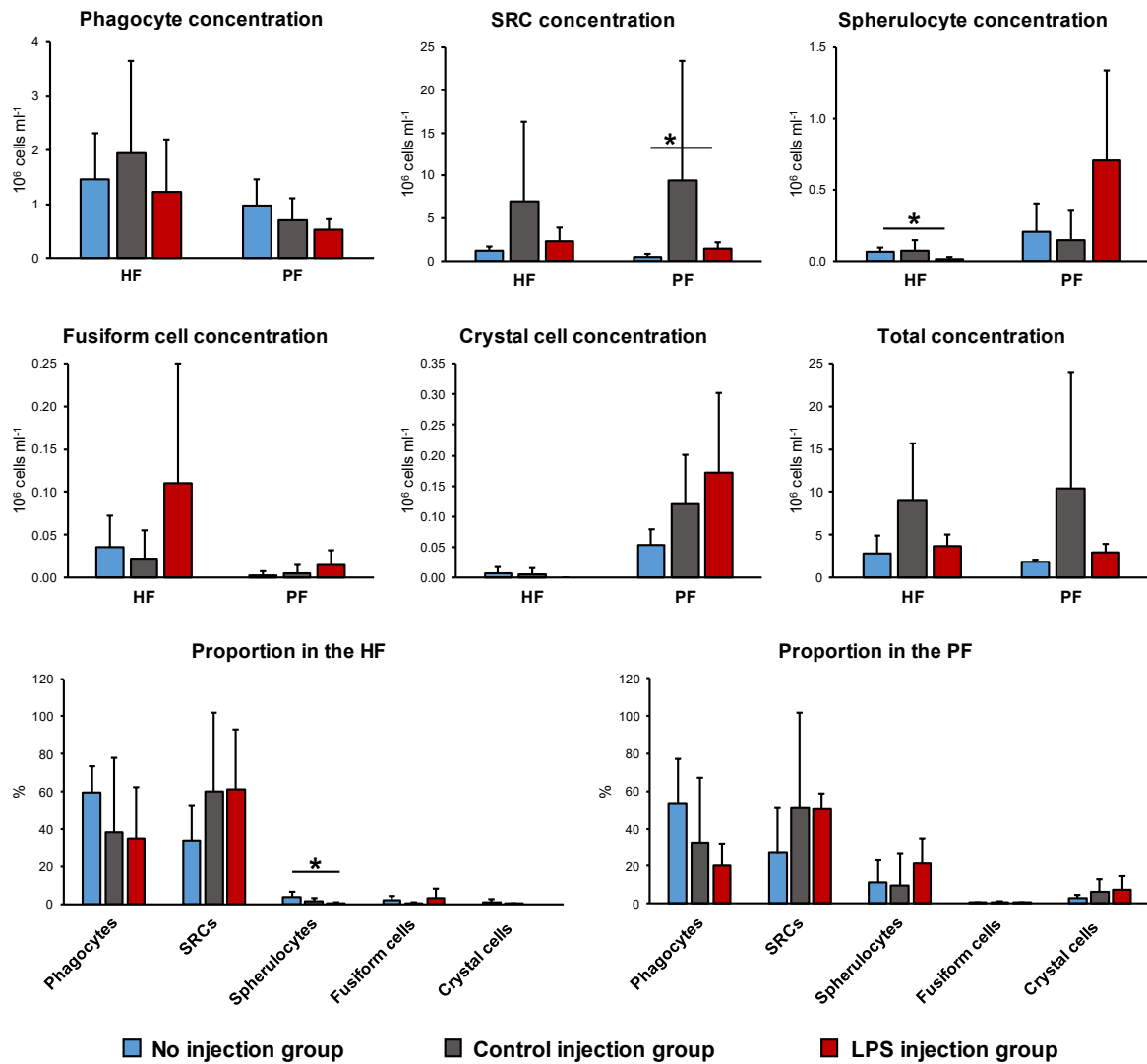
Fig. 5. Cell concentration and proportion fluctuations 24 hours after control and lipopolysaccharide (LPS) injections for each cœlomocyte type in the hydrovascular fluid (HF) and perivisceral fluid (PF). The no injection group received no injection; the control injection group received control injections of sterile seawater; and the LPS injection group received injections of sterile seawater containing lipopolysaccharides (n = 4 in each condition). Results are formulated as mean ± SD and the asterisks (*) represent significative differences (Mann-Whitney test; $p \leq 5\%$)

624 3.2.2. Immune gene expression

625 *3.2.2.1.* De novo *assembly and quality*

626 *assessment*

627 To identify the immune genes in *H. scabra*, the PF cœlomocyte gene expression was

628 compared between LPS injection individuals (test group; n = 3) and control injection

629 individuals (control group; n = 3). The six cDNA libraries sequenced yielded a total of

630 98.34 Gb of bases with a total of raw reads per sample ranging from 87.47 M to 143.07

631 M. After filtering and *de novo* assembling all the samples, we obtained a transcriptome

632 of 162,703 unigenes with a total length of 171,636,263 bp, an average length of 1,054

633 bp, an N50 of 3,241 bp and GC proportion of 38.42%. **Table 3** summarizes the quality

634 metrics of the clean reads and unigenes for each individual transcriptome. The number

635 of unigenes per individual ranged from 85,950 to 101,825 with most of them having a

636 length between 300 and 3000 (**Fig. 6A**).

637 **Table 2.** Quality metrics of clean reads and unigenes for each individual replicate; CON
638 – control injection; LPS – LPS injection; R – replicate number.

Replicates	CON-R1	CON-R2	CON-R3	LPS-R1	LPS-R2	LPS-R3
Reads						
Total raw reads (MB)	124.94	142.15	112.66	143.07	107.81	96.19
Total clean reads (MB)	113.14	128.04	102.82	128.15	96.03	87.46
Total clean bases (GB)	16.97	19.21	15.42	19.22	14.4	13.12
Clean reads Q20 (%)	98.3	98.3	98.3	98.3	98.3	98.3
Clean reads ratio (%)	90.6	90.1	91.3	89.6	89.1	90.02
Unigenes						
Total number	90,695	101,825	85,950	90,020	89,967	86,535
Total length (Mbp)	77.36	81.84	60.41	76.39	69.83	72.21
Mean length (bp)	853	803	702	848	776	834
N50 (bp)	1,610	1,473	1,147	1,668	1,505	1,661
GC (%)	38.4	38.5	38.3	38.5	38.5	38.4

639

Electronic copy available at: https://ssrn.com/abstract=4658658

3.2.2.2.   Completeness   evaluation   and

general functional annotation

642   BUSCOs were evaluated to assess the completeness of individual transcriptomes and

643   the merged transcriptome (**Fig. 6B**). For the individual transcriptomes, the BUSCO

644   percentage ranged from 54.8% (CON-R3) to 76.9% (LPS-R1) of complete BUSCOs

645   (complete and duplicated single copies); from 13.2% (LPS-R1) to 24.2% (CON-R3) of

646   fragmented BUSCOs; and from 8.3% (CON-R1) to 21.0% (CON-R3) of missing

647   BUSCOs. The percentages for the merged transcriptome were 94.5% complete

648   BUSCOs (59.5% complete single copies and 35.0% copies); 3.2% fragmented

649   BUSCOs; and 2.2% missing BUSCOs. While the individual transcriptomes showed

650   variable degrees of completeness, the merged transcriptome showed a low proportion

651   of fragmented and missing BUSCOs (3.2% and 2.2 %, respectively), indicating an

652   overall good assembly quality [15].

653   To obtain a first functional indication, each unigenes were aligned to seven functional

654   databases: 43,976 unigenes (27.03%) matched significantly to at least one database

655   (E-value < 10^{-5}) and 2,899 (1.78%) to the seven databases. Nr was the database that

656   matched the highest number of unigenes with 36,954 annotated unigenes (22.71% of

657   all unigenes), followed by InterPro (29,966; 18.42%) and KEGG (29,518; 18.14%)

658   databases (**Fig. 6C**). For the NR annotation, the species distribution of unigenes was

659   36.98% in *Acanthaster planci*, 25.76% in *Strongylocentrotus purpuratus*, 4.03% in

660   *Saccoglossus kowalevskii*, 2.34% in *A.japonicus* and 30.69% for other species (**Fig.**

661   **6D**). General functional distribution of KOG, GO and KEGG annotations can be

662   consulted in **Supplementary Material 3**.

A. Length distribution

B. BUSCO assessment

C. Annotation distribution

D. Species distribution
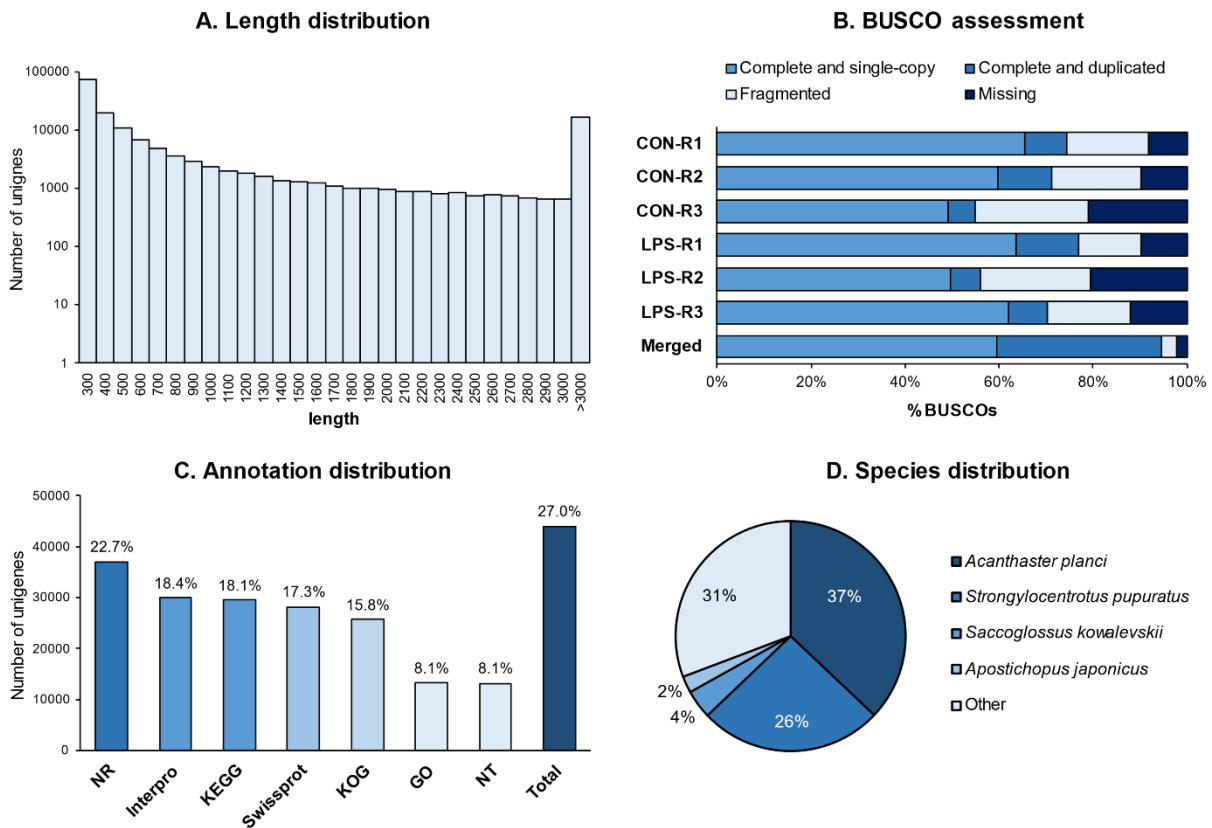
Fig. 6. Quality assessment and functional annotation metrics of the coelomocyte transcriptome of *H.* scabra. A. Length distribution of unigene sequences (in bp; the number of unigenes is embedded in the graph). B. BUCO assessment graph (CON-R – control injection replicates; LPS-R – LPS injection replicates). C. Proportion of annotated unigenes for each functional database (the percentage of annotated unigene is embedded in the graph). D. Species distribution for the Nr annotation with the respective percentage for each species.

3.2.2.3. Identification of differentially

expressed unigenes (DEGs) after the LPS injection

A differential expression analysis was performed to identify the differentially expressed genes (DEGs) between control injection and LPS injection individuals (FDR ≤ 5% and a │$\log_2$ fold change│ ≥ 1). In total, 945 DEGs were obtained (0.77% out of all unigenes), including 673 up-regulated unigenes and 272 down-regulated unigenes in the LPS injection individuals (**Fig. 7A**). A clear positive correlation was found between individual replicates from the same condition and a negative or weak correlation between individuals from the two different conditions (**Fig. 7B)**. Furthermore, the LPS injection

32

681   individuals seemed to have weaker correlation than within the control injection group,

682   suggesting a higher variability in gene expression following the immunological stress.

683   A heatmap was performed based on the expression level of DEGs: the result of the

684   clustering found individual replicates of the same condition gathered and split the

685   unigenes into two clear clusters corresponding to up and down-regulated unigenes

686   (**Fig. 7C**). The number of DEGs 24 hours after an LPS challenge seemed to be variable

687   across sea cucumber species with 1,347 DEGs in *A. japonicus* (890 up-regulated and

688   447 down-regulated; [14]), 7,074 in *H. leucospilota* (666 up-regulated and 6,408 down-

689   regulated; [28]) and 5,524 in *H. forskali* (2,702 up-regulated and 2,822 down-regulated;

690   unpublished data). With 945 DEGs, *H. scabra* appears therefore to display the lower

691   number of DEGs among the sea cucumber species investigated but is the one that

692   shows the maximum ratio of up-regulated/down-regulated genes, namely 2.47.

693   However, it should be noted that the protocol used in the different species was not

694   exactly the same, which could also explain some of the variability in the number of

695   DEGs between species. The full list of DEGs in *H. scabra* can be consulted in

696   **Supplementary Material 4**.

A. Differential expression analysis

Up: 673
Down: 272
Not DEG: 121,807

log10(gene expression level of LPS)

log10(gene expression level of CON)

B. Correlation matrix based on the DEGs

CON-R3
CON-R1
CON-R2
LPS-R3
LPS-R1
LPS-R2

C. Heatmap based on the DEGs

CON-R3 CON-R1 CON-R2 LPS-R3 LPS-R1 LPS-R2

■ Control injection   ■ LPS injection
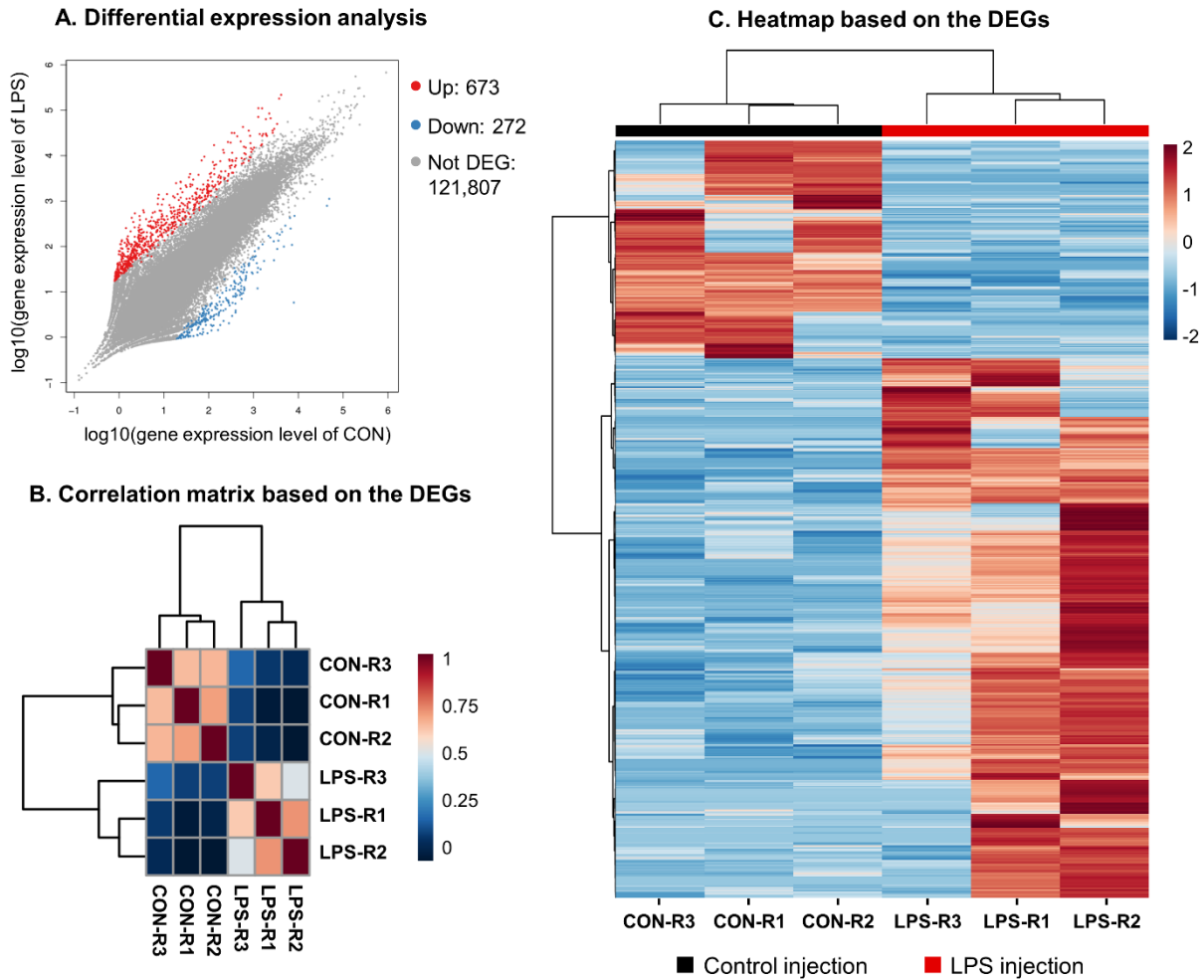
Fig. 7. Differential expression analysis between control and LPS injection individuals in *H. scabra*. A. Scatter plot representation of the differential expression analysis: out of the 122,752 unigenes, 673 were up-regulated (in red; FDR ≤ 5% and $\log_2$ fold change ≥ 1) and 272 were down-regulated (in blue; FDR ≤ 5% and $\log_2$ fold change ≤ -1); the remaining 121,807 were not differentially expressed (in grey; FDR > 5% or/and │$\log_2$ fold change│ < 1). B. Correlation matrix of the individual replicates based on the 945 DEGs. C. Heatmap based on the 945 DEGs: individuals from the same condition are gathered and DEGs are divided into two clusters corresponding to down-regulated unigenes (above) and up-regulated unigenes (below).

3.2.2.4. Functional distribution and enrichment analysis of GO terms and KEGG pathways

Firstly, regarding GO annotations, 160 DEGs were annotated with at least one GO term (16.9%), corresponding to a total of 777 annotations. Among these GO annotations, 325 fell in the category of cellular component, followed by the categories biological process with 251 annotations and molecular function with 201 annotations.

34

Among the most interesting gene ontology related to the immune response, the GO terms "binding" and "catalytic activity" showed 80 and 62 annotations, respectively.

Secondly, regarding KEGG annotations, 363 DEGs matched to at least one pathway (38.4%) corresponding to 1073 pathway annotations that were distributed in the following decreasing order: 336 in human diseases; 263 in organismal systems; 160 in environmental information processing; 146 in metabolism; 126 in cellular process; and 42 in genetic information processing. Among the organismal system categories, the immune system was the most annotated pathway with 64 annotations. The top ten most enriched pathways are shown in **Table 4**: pertussis pathway was the first followed by protein digestion and absorption and legionellosis. Several infectious human disease pathways are represented which is probably explained by many homologies with proteins of the signalling pathways in response to infection. Cytokine-cytokine receptor interaction pathway can also be highlighted; cytokines are known to play a critical function in inflammation and communication between immune cells [29]. Thanks to the KEGG enrichment, we also dressed to the top-ten most enriched pathways within the immune system pathways to identify some important pathways involved in the response to LPS injection. The three most enriched immune pathways were Th17 cell differentiation, NOD-like receptor signalling pathways and IL-17 signalling pathway (**Table 4**). These three pathways are important in immunity: Th17 cells are a subset of T helper pro-inflammatory cells, and their differentiation is mediated by various cytokines [30] that could have some homologues in sea cucumbers; NOD-like receptors are important pathogen recognition receptors [31] and IL-17 is a cytokine involved in the recruitment of immune cells [30]. Other interesting pathways related to immune response were present such as complement and coagulation cascades, Toll and Imd signalling pathway, and Toll-like receptor signalling

35

738　pathway. The complement is an important complex of humoral factors that are involved

739　in numerous immune mechanisms including the opsonisation and the stimulation of

740　the adaptive immune system [4]. Toll-like receptors and Imd signalling cascade

741　participate in the recognition and initiation of the immune response in innate immunity

742　[29]. The detailed results of the GO and KEGG functional enrichment can be consulted

743　in **Supplementary Material 5**.

744　**Table 4.** KEGG functional enrichment analysis: the 10 most enriched pathways in all
745　pathways (A) and immune system pathways (B). The columns "Annotated DEGs" and
746　"Annotated unigenes" represent the number of unigenes (and proportion) that matched
747　the pathway among the lists of DEGs and all the unigenes, respectively.

	Pathway ID	Annotated DEGs	Annotated unigenes	p-value	Pathway
A. All pathways					
1.	**ko05133**	21 (5.79%)	386 (1.31%)	1.72 10^{-8}	Pertussis
2.	**ko04974**	20 (5.51%)	452 (1.53%)	1.02 10^{-6}	Protein digestion and absorption
3.	**ko05134**	16 (4.41%)	340 (1.15%)	5.72 10^{-6}	Legionellosis
4.	**ko05132**	18 (4.96%)	455 (1.54%)	1.62 10^{-5}	Salmonella infection
5.	**ko05164**	21 (5.79%)	599 (2.03%)	2.00 10^{-5}	Influenza A
6.	**ko05200**	43 (11.85%)	1833 (6.21%)	3.85 10^{-5}	Pathways in cancer
7.	**ko04060**	9 (2.48%)	139 (0.47%)	5.87 10^{-5}	Cytokine-cytokine receptor interaction
8.	**ko04510**	29 (7.99%)	1158 (3.92%)	2.58 10^{-4}	Focal adhesion
9.	**ko04972**	13 (3.58%)	343 (1.16%)	3.63 10^{-4}	Pancreatic secretion
10.	**ko04659**	8 (2.2%)	142 (0.48%)	3.89 10^{-4}	Th17 cell differentiation
B. Immune system pathways					
1.	**ko04659**	8 (2.2%)	142 (0.48%)	3.89 10^{-4}	Th17 cell differentiation
2.	**ko04621**	19 (5.23%)	799 (2.71%)	5.09 10^{-3}	NOD-like receptor signaling pathway
3.	**ko04657**	9 (2.48%)	281 (0.95%)	8.37 10^{-3}	IL-17 signaling pathway
4.	**ko04624**	8 (2.2%)	256 (0.87%)	1.44 10^{-2}	Toll and Imd signaling pathway
5.	**ko04610**	6 (1.65%)	177 (0.6%)	2.26 10^{-2}	Complement and coagulation cascades
6.	**ko04611**	10 (2.75%)	476 (1.61%)	7.13 10^{-2}	Platelet activation
7.	**ko04670**	8 (2.2%)	387 (1.31%)	0.106	Leukocyte transendothelial migration
8.	**ko04612**	3 (0.83%)	107 (0.36%)	0.145	Antigen processing and presentation
9.	**ko04658**	10 (2.75%)	583 (1.98%)	0.183	Th1 and Th2 cell differentiation
10.	**ko04620**	4 (1.1%)	246 (0.83%)	0.358	Toll-like receptor signaling pathway

36

3.2.2.5. Identification of immune differentially

749   *expressed unigenes*

750   A total of 80 immune differentially expressed genes (IDEGs) were identified based on

751   KEGG enrichment analysis and keyword research, of which 52 were up-regulated and

752   28 were down-regulated in LPS injection individuals. Among the 64 unigenes that were

753   classified in the general pathway "immune system", 41 were selected based on their

754   relevance to their immune function(s) (64%). The remaining 39 IDEGs were selected

755   by the keyword research based on their annotation that matched immune genes of

756   interest reported in previous studies about echinoderm immunity [4,16,17]. IDEGs

757   were classified into 17 "gene families" that were defined based on presumed immune

758   functions or existing protein families to enhance the readability of the IDEGs list. This

759   list is shown in **Figures 8 and 9** and the full list containing all the unigenes annotated

760   in the immune system pathway, as well as unigenes selected by keyword search, can

761   be consulted in **Supplementary Material 6**.

Annotation	E-value	FDR	FC	Relative expression					
				R1	R2	R3	R1	R2	R3
NLRP10		****	7.89						
		****	7.35						
		****	6.88						
		****	6.82						
		****	6.37						
		***	6.08						
		***	5.82						
		***	5.81						
		**	5.51						
		***	5.27						
		*	5.03						
		**	4.54						
		*	3.83						
		****	-10.42						
		***	-5.67						
		**	-5.22						
		**	-5.09						
		*	-5.01						
		*	-4.95						
		**	-4.54						
		**	-4.34						
NLRP3		****	6.89						
		*	4.54						
		*	-4.74						
		*	-4.68						
		*	-3.79						

E-value: 10^{-5}, 10^{-50}, 0

Rel. Exp.: 1.5, 0, -1.5

■ Control injection   ■ LPS injection

762
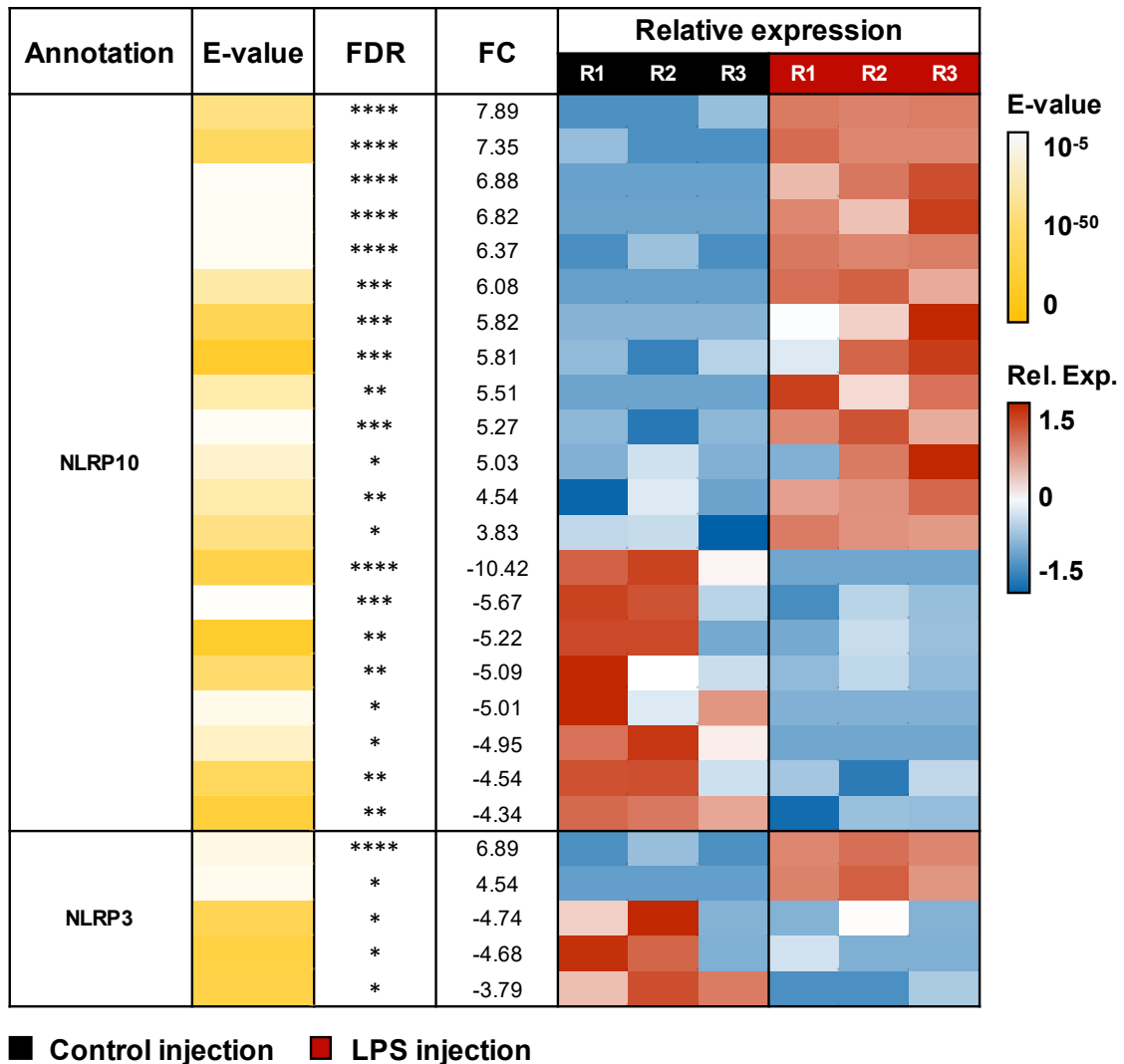
Fig. 8. List of immune differentially expressed unigenes (IDEGs) in the "gene family" of NLRPs (see explanations in the text). For each unigene is provided: the functional annotation (when possible as an abbreviation, the full name is visible in the text or **Supplementary Material 6**); the associated E-value as a colour scale; the false discovery rate (* FDR ≤ 5%; ** FDR ≤ 1%; *** FDR ≤ 0.1%; **** FDR ≤ 0.01%); the FC value (formulated as $\log_2(FC)$: a positive FC means up-regulated and negative FC means down-regulated in LPS injection individuals); the relative expression for each replicate (FPKM transformed by $\log_{10}$ and autoscaled). Among the same gene family, unigenes are ordered from the highest to the lowest FC for up-regulated unigenes, and then from the lowest to the highest for down-regulated unigenes. Legend: FC – fold change; FDR – false discovery rate; LPS injection – lipopolysaccharide injection individuals; R – individual replicate; Rel. Exp. – relative expression.

Gene Family	Annotation	E-value	FDR	FC	Relative expression (Control R1, R2, R3 / LPS R1, R2, R3)
Cytokines and related proteins	Interleukin-17-5		***	6.22	
	IRAK4		***	5.81	
	IFN-induce GTPase 1-like iso. X2		**	5.39	
	Putative interleukin 17-like protein		*	4.70	
	Interleukin-25		**	4.55	
	Interleukin 17-like protein		*	4.12	
	IL1RAP		*	4.02	
	ADAMTS		*	4.01	
	ADAMTS		*	3.75	
	IFN-induce GTPase 1-like		***	-5.83	
Lectins	Lactose-binding lectin I-2 iso. X2		***	5.94	
	C-type lectin d.-c. protein 162		**	5.47	
	Techylectin-5A-like iso. X2		**	4.91	
	Ladderlectin-like		**	4.71	
	Techylectin-5B		**	-5.06	
	Techylectin-5B		**	-4.94	
SVEP1	SVEP1		****	6.89	
	SVEP1 iso. X2		****	6.40	
	SVEP1 iso. X2		****	6.21	
	SVEP1 iso. X2		****	5.99	
	SVEP1		***	5.94	
	SVEP1		***	5.53	
Apoptosis	TNIP3		**	4.69	
	TNIP3		*	3.89	
	SH3BGRL3		**	-5.58	
	FADD protein		*	-4.88	
	BOK		*	-4.08	
Coagulation	Amassin-2 precursor		***	5.07	
	Amassin-2 precursor		***	4.79	
	Coagulation factor VII		***	-5.71	
	Arylsulfatase E		**	-5.04	
	Arylsulfatase B iso. X3		*	-4.46	
Complement	MRC2-like iso. X2		**	4.88	
	MRC2-like iso. X3		*	4.73	
	Complement factor B		*	4.44	
	MMR1-like		*	4.36	
	Ficolin-2-like		**	-5.19	
Integrins	Integrin beta-1-B-like		**	-5.51	
	Integrin beta-1-A		*	-4.45	
	Integrin beta-1-B-like		*	-4.37	
	Integrin beta-1-B-like		*	-3.91	
Heat shock proteins	HSP70		**	5.27	
	HSP26		*	4.86	
	HSP70		*	4.44	
	HSP26		*	4.13	
Antioxidant	PHGPx		*	3.87	
	Glutathione peroxidase		*	3.66	
Epidermal growth factors	Fibropellin-3 iso. X3		*	3.99	
	Fibropellin-3-like		*	-4.37	
Ca²⁺ regulation	CD38-like		****	7.49	
Lysin	Lysozyme		*	-4.89	
Phenoloxidase	Laccase-type phenoloxidase		*	3.51	
SCRC	DMBT1-like		*	4.57	
Tetraspanin	CD63 antigen-like		**	-5.26	

E-value scale: 10^{-5}, 10^{-50}, 0

Rel. Exp. scale: 1.5, 0, -1.5

■ Control injection   ■ LPS injection

Fig. 9. List of immune differentially expressed unigenes (IDEGs). For each unigene is provided: the "gene family"; the functional annotation (when possible as an abbreviation, the full name is visible in the text or **Supplementary Material 6**); the associated E-value as a colour scale; the false discovery rate (* FDR ≤ 5%; ** FDR ≤ 1%; *** FDR ≤ 0.1%; **** FDR ≤ 0.01%); the FC value (formulated as $\log_2$(FC): a positive FC means up-regulated and a negative FC means down-regulated in LPS

39

782 injection individuals); the relative expression for each replicate (FPKM transformed by
783 $\log_{10}$ and autoscaled). Among the same gene family, unigenes are ordered from the
784 highest to the lowest FC for up-regulated unigenes, and then from the lowest to the
785 highest for down-regulated unigenes. Legend: d.-c. – domain-containing; FC – fold
786 change; FDR – false discovery rate; iso. – isoform; LPS injection – lipopolysaccharide
787 injection individual; R – individual replicate; Rel. Exp. – relative expression.

788 The most represented gene family among IDEGs was NLRPs (Nucleotide-binding

789 oligomerization domain, Leucine-rich Repeat and Pyrin domain-containing) with a total

790 of 26 unigenes (**Fig. 8**). Of these, 21 were annotated as NLRP10 and 5 as NLRP3 both

791 in *A. japonicus*. Surprisingly, unigenes that shared the same annotation could be up-

792 regulated or down-regulated: for unigenes annotated as NLRP10, 13 were up-

793 regulated (61.9%) and 8 were down-regulated (38.1%) and for unigenes annotated as

794 NLRP3, 2 were up-regulated (40%) and 3 were down-regulated (60%). It should also

795 be noted that the transcriptome contains 274 unigenes annotated as NLRP10 and 86

796 annotated as NLRP3 that were not differentially expressed. Therefore, 7.1% of

797 unigenes annotated as NLRP10 and 5.5% of unigenes annotated as NLRP3 were

798 differentially expressed. NLRP are members of the NLR family (NOD-like receptors),

799 one of the main categories of pathogen recognition receptors (PRRs), which are known

800 to play an important function in the innate immune system by regulating the

801 inflammation process, promoting the mature form of the cytokines IL-1β and IL-18 and

802 inducing a particular type of programmed cell death called pyroptosis [37]. In the sea

803 cucumber *A. japonicus*, it was demonstrated that both NLRP10 and NLRP3 are

804 involved in the response of bacterial infection: NLRP10 decrease the level of Caspase-

805 1 and MMP37, inhibiting the pyroptosis [32] whereas NLRP3 promotes the

806 inflammation in the same way as described in vertebrates [33]. The large number of

807 unigenes annotated as NLRPs in *H. scabra* may be explained by an expansion of the

808 genes encoding these receptors, as was demonstrated for several immune gene

809 families in the sea urchin genome [17]. Investigations including genomic data are in

40

810 progress to elucidate the reasons for such a diversity of transcripts annotated as

811 NLRPs in holothuroids.

812 The gene family that comes next is cytokines and related proteins, with a total of 10

813 unigenes (**Fig. 9**). Among these, three were annotated as interleukin 17 (interleukin-

814 17-5, interleukin 17-like protein, putative interleukin 17-like protein), two as interferon-

815 induce GTPase 1-like (IFN-induce GTPase 1-like), one as interleukin-1 receptor-

816 associated kinase 4 (IRAK4), one as interleukin 25, one as interleukin-1 receptor

817 accessory protein (IL1RAP) and two as a disintegrin and metalloproteinase with

818 thrombospondin motifs (ADAMTS). All were up-regulated in the LPS injection group

819 except one of the unigenes annotated as IFN-induce GTPase 1-like. Cytokines are

820 important immune proteins that stimulate inflammation and participate in the

821 recruitment of immune cells [29,30]. In sea cucumbers, Wu et al. [28] reported four

822 families of cytokines including BCL/CLL, EPRF1, IL-17 and TSP/TPO among whichIL-

823 17 was the most expressed family 24 hours after an exposition to LPS in the species

824 *H. leucospilota.* In our study, mainly IL-17 family members were identified although two

825 unigenes annotated as ADAMTS thrombospondin-containing motifs (as in TSP/TPO

826 in [28]) and one as BOK, a member of BCL/CLL family (classified in apoptosis gene

827 family in **Fig. 9**). Therefore, our results corroborate the result obtained in *H.*

828 *leucospilota* which suggest that IL-17 cytokines are the most important cytokine family

829 in the holothuroid immune response to bacterial infection.

830 Among IDEGs, six lectins were identified including one lactose-binding lectin, one C-

831 type lectin domain-containing protein 162, one ladderlectin-like and three techylectin-

832 like. Most were up-regulated except two techylectin-like (**Fig. 9**). Lectins are PRRs

833 specialised in the recognition of sugar motifs [4]. In *H. scabra*, a T-antigen-specific

834 lectin was purified from the PF and its agglutinin and antibacterial activity was

41

835 demonstrated against both Gram-negative and Gram-positive bacteria [34]. More

836 recently, it was shown that C-type lectins have also an important function in host

837 defence and that their activity is calcium-dependent in *A. japonicus* [35]. Our results

838 support that lectins are an important component of the innate immune response in sea

839 cucumbers and suggest that a large diversity of lectin types is involved in this response.

840 Six DEGs were annotated as sushi, von Willebrand factor type A, EGF and pentraxin

841 domain-containing protein 1-like (SVEP1-like) and all were up-regulated (**Fig. 9.**).

842 SVEP1 is an extracellular matrix protein that contains several domains including a

843 pentraxin domain [36]. Pentraxins are highly conserved domains that act as PRRs and

844 are involved in the acute innate immune response. More specifically, SVEP1 is mainly

845 known in humans to promote vascular disease because of its interaction with platelet

846 receptors [36]. In sea cucumbers, the overexpression of SVEP1-like suggests that

847 these genes could be involved in the recognition of Gram-negative bacteria and could

848 also act as an agglutinin.

849 Then, five DEGs were presumed to have a function in apoptosis (**Fig. 9**). These

850 comprise two unigenes annotated as tumour necrosis factor-α induced protein 3

851 interacting protein 3-like (TNFAIP3 interacting protein or TNIP3-like), one annotated

852 as SH3 domain-binding glutamic acid-rich-like protein 3 (SH3BGRL3), one annotated

853 as FAS-associated death domain protein (FADD protein), and one annotated as BCL-

854 2-related ovarian killer protein (BOK). While unigenes annotated as TNIP3 were up-

855 regulated, other unigenes involved in apoptosis were down-regulated. It was shown

856 that TNIP3 is an inhibitor of the nuclear factor-kappa B (NF-κB) activation that

857 promotes inflammation and inhibits apoptosis [37]; SH3BGRL3 was described as an

858 inhibitor of the tumour necrosis factor α (TNF-α) [38]; FADD protein promotes the

859 apoptosis by playing the function of adaptor for tumour necrosis factor receptors, and

42

860　this function was demonstrated in sea cucumbers [39]; and BOK is a pro-apoptotic

861　member of the BCL-2 family [40]. The differential expression of all these unigenes

862　shows contradicting effects (*i.e.* activation and inhibition of apoptosis at the same time)

863　suggesting a fine regulation of apoptosis 24 hours after the LPS injection in *H. scabra*.

864　Five DEGs were identified to participate in the coagulation processes, namely two

865　unigenes annotated as amassin-2 precursor, two unigenes annotated as arylsulfatase

866　(E and B) and one unigene annotated as coagulation factor VII (**Fig. 9**). Amassin is a

867　secreted plasmatic protein that was first identified in sea urchins to play a critical

868　function in cœlomocyte aggregation by forming extracellular bridges of disulphide

869　bonds between cells when polymerising [41]. However, the protein linking the cells to

870　the amassin complex was not identified. Later, D'Andrea-Winslow et al. [42]

871　demonstrated the importance of arylsulfatase in clotting and proposed that this protein

872　could be the extracellular membrane protein responsible for this link between

873　cœlomocyte and amassin bridges. While amassin-precursors are strongly up-

874　regulated in our results, arylsulfatase E and B are down-regulated, casting doubt on

875　this hypothesis of a possible interaction or at least suggesting that these two genes

876　are not necessarily co-expressed. The amassin-precursor expression was already

877　identified in the sea cucumber *A. japonicus* but surprisingly in this species, the

878　unigenes coding for amassin precursors were down-regulated at 24-, 48- and 72-hours

879　post LPS injections [12]. Regarding the unigene annotated as coagulation factor VII,

880　in contrast to the majority of other unigenes that matched genes from echinoderm

881　genomes, the unigenes coding for the coagulation factor VII matched the genome of

882　*Mus musculus* (see complete annotations in **Supplementary Material 6**). In

883　vertebrates, this particular serine protease has a critical function in coagulation by

884　initiating the coagulation cascade when encountering tissue damage [43]. This protein

43

885 was rarely reported in echinoderms; it was only shown that a low-density lipoprotein-

886 receptor-related protein 4 precursor of the genome of the sea urchin

887 *Strongylocentrotus purpuratus* shared 34% of identity with serine protease sequences

888 in humans [43]. In our results, while Nr annotation results in "low-density lipoprotein

889 receptor-related protein 4-like [*Acanthaster planci*]" (E-value = 5.5 10^{-51}), SwissProt

890 annotation results in "Coagulation factor VII OS=*Mus musculus* GN=F7 PE=1 SV=1"

891 (E-value = 5.2 10^{-43}), suggesting that the genome of *H. scabra* share the same identity

892 with coagulation factor VII as *S. purpuratus*. In addition, serine proteases are known to

893 participate in an enzymatic cascade that leads to the maturation of prophenoloxidase

894 into active phenoloxidase in arthropods, the enzyme responsible for melanisation [24].

895 Here, more than highlighting its presence in the transcriptome of *H. scabra*, we have

896 shown that this unigene is down-regulated after the LPS injection, suggesting it could

897 have a function in the response to immunological stress in echinoderms as well.

898 Five DEGs were identified for their involvement in the complement system. They

899 include two unigenes annotated as C-type mannose receptor 2-like (MRC2-like), one

900 annotated as complement factor B, one as macrophage mannose receptor 1-like

901 (MMR1-like), and one annotated as ficolin-2-like (**Fig. 9**). Since the first homologue to

902 the component C3 was identified in sea urchins, many other homologues have been

903 discovered [4], including in sea cucumbers [14]. In vertebrates, activation of this system

904 leads to various immune mechanisms including phagocytosis, lysis and inflammation

905 [4]. The study by Dong et al. [12] showed that in *A. japonicus*, immunostimulation with

906 LPS led to the overexpression of factor C3 and factor B in cœlomocytes. In our study,

907 while unigenes annotated as factor B and as mannose-binding receptors were

908 overexpressed, unigenes annotated as ficolin-2 homologue were underexpressed

909 after injection of LPS. These results suggest a potential activation of the complement

44

910   system by the lectin-type activation pathway and more specifically by that involving

911   mannose receptors in the presence of LPS. However, it should be noted that in the

912   transcriptome of *H. scabra*, five unigenes were annotated as complement component

913   C3 in *A. japonicus*, but all these unigenes were not differentially expressed (FDR > 5%

914   or/and │$\log_2$ fold change│ < 1). An explanation for this could be that the peak of

915   complement system response occurs before 24 hours in *H. scabra*.

916   The next gene family was integrin with three DEGs annotated as integrin beta-1-B and

917   one annotated as integrin beta-1-A (**Fig. 9**). The four unigenes were down-regulated

918   following the LPS injection. Integrins are transmembrane proteins mostly known to

919   have a function in cell adhesion and attachment to the extracellular matrix [44]. In sea

920   cucumbers, Wang et al. [45] demonstrated that β-integrin was down-regulated in

921   cœlomocytes after an LPS challenge. Interestingly, silencing β-integrin has as a

922   consequence to promote cœlomocyte apoptosis via a β-integrin/focal adhesion kinase

923   (FAK)/ caspase-3 pathway [60]. Our results corroborate those obtained by Wang et al.

924   [45]; the underexpression of integrin beta-1-B and A in *H. scabra* suggests that

925   apoptosis was promoted by this pathway 24 hours after the injection of LPS.

926   Four unigenes annotated as heat shock protein (HSP) were up-regulated and

927   comprised two unigenes annotated as HSP70 and two others annotated as HSP26

928   (**Fig. 9**). HSP family members are highly conserved proteins which have the function

929   of chaperones, *i.e.* they help other proteins to acquire a proper conformation [46]. It

930   was also reported that some HSPs such as HSP70 can act as an activator of the innate

931   immune system by playing the function of danger-signalling molecules [46]. In sea

932   cucumbers, the overexpression of HSP was shown in various contexts of stress

933   including thermal stress [47] but also after an immunostimulation with *V. splendidus* or

934   LPS ([11] and [12], respectively) which could suggest that HSP70 has also this

935   inflammatory effect in sea cucumbers. Regarding HSP26, its overexpression was

936   demonstrated under heat shock experiments in sea cucumbers [47], but the fact our

937   results show its overexpression in response to the LPS injection suggests that they

938   could also be involved in the response to immunological stress.

939   Then, two DEGs coding for proteins having an antioxidant activity were identified, they

940   were annotated as phospholipid hydroperoxide glutathione peroxidase (PHGPx) and

941   glutathione peroxidase (GPx), and both were up-regulated following the LPS injection

942   (**Fig. 9**). GPx constitute a protein family capable of reducing peroxides, hence their

943   antioxidant activity [48]. Peroxides are highly reactive compounds that are notably

944   produced by immune cells to degrade pathogens in a process called a respiratory

945   burst, but this process can also cause oxidative damage to the host tissues if not well-

946   regulated [48]. Therefore, the overexpression of PHGPx and GPx under immunological

947   stress in *H. scabra* could be a regulation process after the release of reactive oxygen

948   species (ROS) during the acute immune response. This function of GPx is for example

949   known to occur after the melanisation process in arthropods [24].

950   Two DEGs were annotated as fibropellin 3 (fibropellin 3 and fibropellin 3-like), of which

951   one was up-regulated and the other was down-regulated (**Fig. 9**). Fibropellins are a

952   family of extracellular matrix proteins that contain repeated epidermal growth factor-

953   like motifs. It was first described as constituting the apical lamina of sea urchin embryos

954   [49]. In the sea cucumber *A. japonicus*, fibropellin was later reported to have a function

955   in regeneration, notably after evisceration [49]. Therefore, the differential expression

956   of fibropellin could suggest that immunological stress can involve mechanisms of

957   tissue regeneration in *H. scabra*.

958 Finally, five DEGs were classified in their own gene family: they comprise ADP-ribosyl

959 cyclase/cyclic ADP-ribose hydrolase 1-like (CD38-like), Lysozyme, Laccase-type

960 phenoloxidase, deleted in malignant brain tumours 1 protein-like (DMBT1-like), and

961 tetraspanin (CD63-like) (**Fig. 9**).

962 CD38 is a transmembrane protein that, upon interaction with the proper ligand, can

963 mobilise the intracellular reserve of calcium cations (Ca^{2+}) [50]. Divalent cations such

964 as Ca^{2+} and Mg^{2+} are important mediators of the immune response and regulate a large

965 spectrum of mechanisms including aggregation and inflammation [13,42]. CD38-like

966 was up-regulated following the LPS injection which can be attributed to the Ca^{2+}

967 release as a signal to stimulate the immune response in *H. scabra*.

968 The DEG annotated as lysozyme was underexpressed in the LPS injection group.

969 These proteins are members of lysins (*i.e.* humoral factors that possess a lytic activity)

970 and are known to break the links between N-acetylmuramic acid and N-

971 acetylglucosamine in the peptidoglycans that constitute the wall of bacteria [29]. They

972 are particularly active against Gram-positive bacteria because Gram-negative bacteria

973 have an outer membrane containing LPS, which is not present in Gram-positive

974 bacteria, making the peptidoglycan layer less easily accessible [29]. We could

975 therefore hypothesise that the presence of LPS, mimicking the presence of Gram-

976 negative bacteria, does not lead to greater production of lysozyme.

977 The DEG annotated as laccase-type phenoloxidase was overexpressed in the LPS

978 injection group. The phenoloxidase constitutes the key component of the melanisation

979 cascade, an important mechanism in innate immunity that was initially described in

980 arthropods [24], but whose presence was then demonstrated in many other taxa [51].In

981 the sea cucumber *A. japonicus*, it was shown that the expression of a laccase-type

47

982 phenoloxidase was the highest in cœlomocytes compared to different other tissues,

983 and was enhanced under immunostimulation with LPS, peptidoglycans and Zymosan

984 A and PolyI:C; and was maximal 24 hours after the exposition to these different

985 immunostimulants, except for peptidoglycans for which the peak occur 12 hours after

986 the immunostimulation [52]. Therefore, our results strongly corroborate the results

987 obtained in *A. japonicus* and support the assumption that phenoloxidase is an

988 important actor of humoral immunity at the scale of Holothuroidea.

989 The DEG annotated as DMBT1-like was overexpressed in the LPS injection group.

990 DMBT1 is a glycoprotein that contains multiple scavenger receptor cysteine-rich

991 (SRCR) domains, which are known to have a function of PRRs [11]. In *A. japonicus*, it

992 was shown that DMBT1-like was up-regulated 24 hours after an immunostimulation

993 with *V. splendidus* in the cœlomocytes from the PF but not in cœlomocytes from the

994 HF [11,53]. These results are consistent with those found in *H. scabra* and suggest

995 that DMBT1-like is an important PRR of Gram-negative bacteria or LPS.

996 The DEG annotated as CD63 antigen-like was down-regulated in the LPS injection

997 group. CD63 is a transmembrane protein which is more associated with late

998 endosomes and lysosomes but which can also be present on the cell surface

999 membrane. It participates in a large spectrum of cellular mechanisms including cell

1000 activation, cell adhesion and cell differentiation [54]. While the functions of a

1001 homologue to CD63 in the immune response have never been demonstrated yet in an

1002 echinoderm, in insects it was shown that the interaction of integrin/tetraspanin had an

1003 effect to activate hemocytes, which represent the equivalent of coelomocytes, but in

1004 arthropods [54]. As in our results, the unigenes coding for integrin-beta-1 and CD63

1005 antigen-like are all down-regulated in the LPS injection group, we could hypothesise

1006 that this activation system is also present in *H. scabra*, the underexpression in treated

48

1007 individuals being likely the result of a retro-control 24 hours after the immunological
1008 stress.

1009   3.2.3. Relation between cœlomocyte populations and gene expression

1010 Studies of gene expression in holothuroids often considered cœlomocytes as an entity,

1011 neglecting the cell type heterogeneity that constitutes this entity (*e.g.* [11,12,28]). In

1012 this way, the differential gene expression is generally considered as the result of an

1013 expression shift in cœlomocytes but could also be the result of a shift in cell populations

1014 with a stable gene expression. In practice, both effects probably influence gene

1015 expression results, but the fact is that gene expression and cell population modification

1016 are rarely assessed at the same time. Recently, it was shown that cœlomocytes from

1017 the PF and the HF of *A. japonicus* have a divergent expression of some immune genes,

1018 the two fluids having different proportions in cell populations [53]. Furthermore, Yu et

1019 al. [55] demonstrated that two subsets of cells from the PF, namely spherical cells and

1020 lymphocyte-like cells, had their own gene expression. These two examples prove that

1021 assessing the change in cell populations is crucial for interpreting the transcriptomics

1022 analysis as well as other types of omics analyses.

1023 Moreover, the cell heterogeneity could in part explain some contradictory results

1024 obtained in some pathways. For instance, regarding unigenes related to apoptosis,

1025 some results suggested that apoptosis was promoted (*e.g.* up-regulation of TNIP3 and

1026 down-regulation of integrin beta-1-B and integrin beta-1-A) while others suggested that

1027 it was inhibited (down-regulation of BOK and FADD). There is a possibility that

1028 apoptosis was promoted in some cœlomocyte populations (*e.g.* activated phagocytes)

1029 while inhibited in others (*e.g.* PCRI), resulting in an overall conflicting effect.

49

1030   Here, the transcriptomic analysis focused on the comparison between control injection

1031   and LPS injection individuals to avoid an "injection stress effect". Despite high inter-

1032   individual variability, the proportions of coelomocyte populations were similar between

1033   these two conditions compared with the non-injected group. This suggests therefore

1034   that the variability in gene expression is mainly due to a shift in gene expression rather

1035   than a shift in cell populations. Unfortunately, it was not possible to estimate directly

1036   the proportion of the different coelomocyte populations in the sequenced samples due

1037   to logistical limitations related to the working field in Madagascar, but it would be

1038   interesting to take this into account in future analyses. Furthermore, the ideal tool for

1039   assessing the sample heterogeneity would be single-cell RNA sequencing, but using

1040   this tool requires many resources, including a high-quality genome to annotate the

1041   results, and would be, therefore, more likely to be carried out firstly on model

1042   echinoderm species (*e.g. S. purpuratus* or *A. japonicus*).

1043   3.2.4. Inter-individual variability in the immune response *H. scabra*

1044   Overall, our results showed a particularly high interindividual variability, especially for

1045   cell concentration and proportions. This high variability can be explained by several

1046   factors including the sex, the age, and the life story of the animal. Unfortunately, it was

1047   impossible to determine the sex in our experiment due to the lack of sexual dimorphism

1048   in *H. scabra*. Regarding the age and the life history, although these phenotypic factors

1049   cannot be totally under control, specimens of *H. scabra* used for the experimentations

1050   came from the same aquaculture pens and were born in the same hatcheries. Over

1051   their growth, they followed the same rearing process and were divided into different

1052   enclosures as a function of their size. Therefore, we could expect that individuals

1053   collected from the same sea pen were similarly aged. Finally, the high interindividual

1054   variability encountered in *H. scabra* is not an exception and was observed in other sea

50

cucumber species (*e.g. H. polii* [20], *A. japonicus* [19], *C. frondosa* [5]) as well as in other echinoderm classes (*e.g. Paracentrotus lividus* [26]). This variability suggests a highly reactive immune system implicating complex regulatory systems in echinoderms.

4. Conclusion

This study describes the different molecular and cellular components of the immune system in the aquacultivated and endangered species *H. scabra*. Five main cell types were described in the HF and PF including, in order of decreasing proportion, phagocytes, SRCs, spherulocytes, fusiform cells and crystal cells. No clear relation was found in the cell population between the two fluids. The injection of LPS and sterile seawater showed mainly a tendency of a decrease in phagocyte proportion concomitant with an increase of SRC proportion in both fluids that would be explained by the recruitment of stem cells to replace the utilisation of immune active cells. Finally, the gene expression analysis of cœlomocytes from the PF 24 hours following LPS injections showed the differential expression of a large number of unigenes involved in highly diverse immune mechanisms.

All these results emphasise the high complexity of the immune system in *H. scabra* and will be useful to better understand its biology in the context of aquaculture as well as provide interesting data for comparative immunology.

5. Acknowledgements

51

1082 ## 6.   Author contributions

1083   **Noé Wambreuse:** Conceptualisation, Formal analysis, Methodology, Writing the

1084   original draft, Writing - review and editing. **Guillaume Caulier:** Conceptualisation,

1085   Writing - review and editing, Supervision. **Igor Eeckhaut:** Conceptualisation, Writing -

1086   review and editing, Project administration, Funding acquisition, Supervision. **Laura**

1087   **Borrello:** Conceptualisation, Methodology, Formal analysis. **Fabrice Bureau:**

1088   Conceptualisation, Writing - review and editing, Project administration, Funding

1089   acquisition, Supervision. **Laurence Fievez:** Conceptualisation, Writing - review and

1090   editing. **Jérôme Delroisse:** Conceptualisation, Formal analysis, Methodology, Writing

1091   - review and editing, Supervision.

1092 ## 7.   Declaration of competing interest

1093   The authors declare that they have no known competing financial interests or personal

1094   relationships that could influence the work reported in this paper.

1095 ## 8.   References

1096   [1]   S.W. Purcell, Value, Market Preferences and Trade of Beche-De-Mer from
1097   Pacific Island Sea Cucumbers, PLoS ONE. 9 (2014) e95075.
1098   https://doi.org/10.1371/journal.pone.0095075.
1099   [2]   J.-F. Hamel, I. Eeckhaut, C. Conand, J. Sun, G. Caulier, A. Mercier, Global
1100   knowledge on the commercial sea cucumber *Holothuria scabra*, in: Adv. Mar.
1101   Biol., Elsevier, 2022: pp. 1–286. https://doi.org/10.1016/bs.amb.2022.04.001.
1102   [3]   J. Delroisse, K. Van Wayneberghe, P. Flammang, D. Gillan, P. Gerbaux, N.
1103   Opina, G.G.B. Todinanahary, I. Eeckhaut, Epidemiology of a SKin Ulceration
1104   Disease (SKUD) in the sea cucumber *Holothuria scabra* with a review on the
1105   SKUDs in Holothuroidea (Echinodermata), Sci. Rep. 10 (2020) 22150.
1106   https://doi.org/10.1038/s41598-020-78876-0.
1107   [4]   L.C. Smith, V. Arizza, M.A. Barela Hudgell, G. Barone, A.G. Bodnar, K.M.
1108   Buckley, V. Cunsolo, N.M. Dheilly, N. Franchi, S.D. Fugmann, R. Furukawa, J.

52

Garcia-Arraras, J.H. Henson, T. Hibino, Z.H. Irons, C. Li, C.M. Lun, A.J. Majeske, M. Oren, P. Pagliara, A. Pinsino, D.A. Raftos, J.P. Rast, B. Samasa, D. Schillaci, C.S. Schrankel, L. Stabili, K. Stensväg, E. Sutton, Echinodermata: The Complex Immune System in Echinoderms, in: E.L. Cooper (Ed.), Adv. Comp. Immunol., Springer International Publishing, Cham, 2018: pp. 409–501. https://doi.org/10.1007/978-3-319-76768-0_13.

[5] G. Caulier, J.-F. Hamel, A. Mercier, From Coelomocytes to Colored Aggregates: Cellular Components and Processes Involved in the Immune Response of the Holothuroid *Cucumaria frondosa*, Biol. Bull. 239 (2020) 95–114. https://doi.org/10.1086/710355.

[6] M.G. Eliseikina, T.Yu. Magarlamov, Coelomocyte Morphology in the Holothurians *Apostichopus japonicus* (Aspidochirota: Stichopodidae) and *Cucumaria japonica* (Dendrochirota: Cucumariidae), Russ. J. Mar. Biol. 28 (2002) 197–202. https://doi.org/10.1023/A:1016801521216.

[7] K. Xing, H. Yang, M. Chen, Morphological and ultrastructural characterization of the coelomocytes in *Apostichopus japonicus*, Aquat. Biol. 2 (2008) 85–92. https://doi.org/10.3354/ab00038.

[8] H.R. Hetzel, Studies on Holothurian Coelomocytes. I. A Survey of Coelomocyte Types, Biol. Bull. 125 (1963) 289–301. https://doi.org/10.2307/1539404.

[9] Y. Prompoon, W. Weerachatyanukul, B. Withyachumnarnkul, Lectin-Based Profiling of Coelomocytes in *Holothuria scabra* and Expression of Superoxide Dismutase in Purified Coelomocytes, Zoolog. Sci. 32 (2015) 345. https://doi.org/10.2108/zs140285.

[10] R.A. Oomen, J.A. Hutchings, Transcriptomic responses to environmental change in fishes: Insights from RNA sequencing, FACETS. 2 (2017) 610–641. https://doi.org/10.1139/facets-2017-0015.

[11] Q. Gao, M. Liao, Y. Wang, B. Li, Z. Zhang, X. Rong, G. Chen, L. Wang, Transcriptome Analysis and Discovery of Genes Involved in Immune Pathways from Coelomocytes of Sea Cucumber (*Apostichopus japonicus*) after *Vibrio splendidus* Challenge, Int. J. Mol. Sci. 16 (2015) 16347–16377. https://doi.org/10.3390/ijms160716347.

[12] Y. Dong, H. Sun, Z. Zhou, A. Yang, Z. Chen, X. Guan, S. Gao, B. Wang, B. Jiang, J. Jiang, Expression Analysis of Immune Related Genes Identified from the Coelomocytes of Sea Cucumber (*Apostichopus japonicus*) in Response to LPS Challenge, Int. J. Mol. Sci. 15 (2014) 19472–19486. https://doi.org/10.3390/ijms151119472.

[13] L.C. Smith, T.S. Hawley, J.H. Henson, A.J. Majeske, M. Oren, B. Rosental, Methods for collection, handling, and analysis of sea urchin coelomocytes, in: Methods Cell Biol., Elsevier, 2019: pp. 357–389. https://doi.org/10.1016/bs.mcb.2018.11.009.

[14] Z.C. Zhou, Y. Dong, H.J. Sun, A.F. Yang, Z. Chen, S. Gao, J.W. Jiang, X.Y. Guan, B. Jiang, B. Wang, Transcriptome sequencing of sea cucumber (*Apostichopus japonicus*) and the identification of gene-associated markers, Mol. Ecol. Resour. 14 (2014) 127–138. https://doi.org/10.1111/1755-0998.12147.

[15] F.A. Simão, R.M. Waterhouse, P. Ioannidis, E.V. Kriventseva, E.M. Zdobnov, BUSCO: assessing genome assembly and annotation completeness with single-copy orthologs, Bioinformatics. 31 (2015) 3210–3212. https://doi.org/10.1093/bioinformatics/btv351.

[16] Z. Xue, H. Li, X. Wang, X. Li, Y. Liu, J. Sun, C. Liu, A review of the immune molecules in the sea cucumber, Fish Shellfish Immunol. 44 (2015) 1–11. https://doi.org/10.1016/j.fsi.2015.01.026.

[17] T. Hibino, M. Loza-Coll, C. Messier, A.J. Majeske, A.H. Cohen, D.P. Terwilliger, K.M. Buckley, V. Brockton, S.V. Nair, K. Berney, S.D. Fugmann, M.K. Anderson, Z. Pancer, R.A. Cameron, L.C. Smith, J.P. Rast, The immune gene repertoire encoded in the purple sea urchin genome, Dev. Biol. 300 (2006) 349–365. https://doi.org/10.1016/j.ydbio.2006.08.065.

[18] F.S. Chia, J. Xing, Echinoderm coelomocytes, Zool. Stud. 35 (1996) 231–254.

[19] Q. Li, R. rong Qi, Y. nan Wang, S. gen Ye, G. Qiao, H. Li, Comparison of cells free in coelomic and water-vascular system of sea cucumber, *Apostichopus japonicus*, Fish Shellfish Immunol. 35 (2013) 1654–1657. https://doi.org/10.1016/j.fsi.2013.07.020.

[20] C. Canicatti, G. D'Ancona, E. Farina- Lipari, The coelomocytes of *Holothuria polii* (Echinodermata). I. light and electron microscopy, Bolletino Zool. 56 (1989) 29–36. https://doi.org/10.1080/11250008909355618.

[21] V. Queiroz, M. Mauro, V. Arizza, M.R. Custódio, M. Vazzana, The use of an integrative approach to identify coelomocytes in three species of the genus *Holothuria* (Echinodermata), Invertebr. Biol. 141 (2022). https://doi.org/10.1111/ivb.12357.

[22] G. Caulier, S. Jobson, N. Wambreuse, J. Delroisse, I. Eeckhaut, A. Mercier, J.-F. Hamel, Vibratile cells and hemocytes in sea cucumbers - clarifications and new paradigms, in: World Sea Cucumbers, Academic Press, EDS.

[23] Q. Li, Y. Ren, L. Luan, J. Zhang, G. Qiao, Y. Wang, S. Ye, R. Li, Localization and characterization of hematopoietic tissues in adult sea cucumber, *Apostichopus japonicus*, Fish Shellfish Immunol. 84 (2019) 1–7. https://doi.org/10.1016/j.fsi.2018.09.058.

[24] I.M. Dubovskiy, N.A. Kryukova, V.V. Glupov, N.A. Ratcliffe, Encapsulation and nodulation in insects, Invertebr. Surviv. J. (2016) 229-246 Pages. https://doi.org/10.25431/1824-307X/ISJ.V13I1.229-246.

[25] S. Jobson, J.-F. Hamel, A. Mercier, Rainbow bodies: Revisiting the diversity of coelomocyte aggregates and their synthesis in echinoderms, Fish Shellfish Immunol. 122 (2022) 352–365. https://doi.org/10.1016/j.fsi.2022.02.009.

[26] V. Matranga, G. Toia, R. Bonaventura, W.E.G. Müller, Cellular and biochemical responses to environmental and experimentally induced stress in sea urchin coelomocytes, Cell Stress Chaperones. 5 (2000) 113. https://doi.org/10.1379/1466-1268(2000)005<0113:CABRTE>2.0.CO;2.

[27] J. Hamel, J. Sun, B.L. Gianasi, E.M. Montgomery, E.L. Kenchington, B. Burel, S. Rowe, P.D. Winger, A. Mercier, Active buoyancy adjustment increases dispersal potential in benthic marine animals, J. Anim. Ecol. 88 (2019) 820–832. https://doi.org/10.1111/1365-2656.12943.

[28] X. Wu, T. Chen, D. Huo, Z. Yu, Y. Ruan, C. Cheng, X. Jiang, C. Ren, Transcriptomic analysis of sea cucumber (*Holothuria leucospilota*) coelomocytes revealed the echinoderm cytokine response during immune challenge, BMC Genomics. 21 (2020) 306. https://doi.org/10.1186/s12864-020-6698-6.

[29] M. Chiaramonte, R. Russo, The echinoderm innate humoral immune response, Ital. J. Zool. 82 (2015) 300–308. https://doi.org/10.1080/11250003.2015.1061615.

1206   [30] T. Korn, E. Bettelli, M. Oukka, V.K. Kuchroo, IL-17 and Th17 Cells, Annu. Rev.
1207   Immunol. 27 (2009) 485–517.
1208   https://doi.org/10.1146/annurev.immunol.021908.132710.
1209   [31] E. Meunier, P. Broz, Evolutionary Convergence and Divergence in NLR Function
1210   and Structure, Trends Immunol. 38 (2017) 744–757.
1211   https://doi.org/10.1016/j.it.2017.04.005.
1212   [32] L.X. Li, X.H. Liu, H. Wang, L. Wang, B. Han, Y.Q. Chang, J. Ding, Molecular
1213   characterization and expression of NLRP10 in the antibacterial host defense of
1214   the sea cucumber (*Apostichopus japonicus*), Gene. 675 (2018) 110–118.
1215   https://doi.org/10.1016/j.gene.2018.06.072.
1216   [33] Z. Lv, Z. Wei, Z. Zhang, C. Li, Y. Shao, W. Zhang, X. Zhao, Y. Li, X. Duan, J.
1217   Xiong, Characterization of NLRP3-like gene from *Apostichopus japonicus*
1218   provides new evidence on inflammation response in invertebrates, Fish Shellfish
1219   Immunol. 68 (2017) 114–123. https://doi.org/10.1016/j.fsi.2017.07.024.
1220   [34] N.M. Gowda, U. Goswami, M. Islam Khan, T-antigen binding lectin with
1221   antibacterial activity from marine invertebrate, sea cucumber (*Holothuria
1222   scabra*): Possible involvement in differential recognition of bacteria, J. Invertebr.
1223   Pathol. 99 (2008) 141–145. https://doi.org/10.1016/j.jip.2008.04.003.
1224   [35] X. Wei, X. Liu, J. Yang, S. Wang, G. Sun, J. Yang, Critical roles of sea
1225   cucumber C-type lectin in non-self recognition and bacterial clearance, Fish
1226   Shellfish Immunol. 45 (2015) 791–799. https://doi.org/10.1016/j.fsi.2015.05.037.
1227   [36] J.S. Elenbaas, U. Pudupakkam, K.J. Ashworth, C.J. Kang, V. Patel, K. Santana,
1228   I.-H. Jung, P.C. Lee, K.H. Burks, J.M. Amrute, R.P. Mecham, C.M. Halabi, A.
1229   Alisio, J. Di Paola, N.O. Stitziel, SVEP1 is an endogenous ligand for the orphan
1230   receptor PEAR1, Nat. Commun. 14 (2023) 850. https://doi.org/10.1038/s41467-
1231   023-36486-0.
1232   [37] L. Verstrepen, I. Carpentier, R. Beyaert, The Biology of A20-Binding Inhibitors of
1233   NF-κB Activation (ABINS), in: C. Ferran (Ed.), Mult. Ther. Targets A20, Springer
1234   New York, New York, NY, 2014: pp. 13–31. https://doi.org/10.1007/978-1-4939-
1235   0398-6_2.
1236   [38] C. Xu, P. Zheng, S. Shen, Y. Xu, L. Wei, H. Gao, S. Wang, C. Zhu, Y. Tang, J.
1237   Wu, Q. Zhang, Y. Shi, NMR structure and regulated expression in APL cell of
1238   human SH3BGRL3, FEBS Lett. 579 (2005) 2788–2794.
1239   https://doi.org/10.1016/j.febslet.2005.04.011.
1240   [39] Y. Wang, J. Diao, B. Wang, X. Xu, M. Gui, C. Li, M. Guo, A second FADD
1241   mediates coelomocyte apoptosis response to *Vibrio splendidus* infection in sea
1242   cucumber *Apostichopus japonicus*, Fish Shellfish Immunol. 127 (2022) 396–404.
1243   https://doi.org/10.1016/j.fsi.2022.06.046.
1244   [40] J.M. Rodriguez, M.A. Glozak, Y. Ma, W.D. Cress, Bok, Bcl-2-related Ovarian
1245   Killer, Is Cell Cycle-regulated and Sensitizes to Stress-induced Apoptosis, J.
1246   Biol. Chem. 281 (2006) 22729–22735. https://doi.org/10.1074/jbc.M604705200.
1247   [41] B.J. Hillier, V.D. Vacquier, Amassin, an olfactomedin protein, mediates the
1248   massive intercellular adhesion of sea urchin coelomocytes, J. Cell Biol. 160
1249   (2003) 597–604. https://doi.org/10.1083/jcb.200210053.
1250   [42] L. D'Andrea-Winslow, D.W. Radke, T. Utecht, T. Kaneko, K. Akasaka, Sea
1251   urchin coelomocyte arylsulfatase: a modulator of the echinoderm clotting
1252   pathway, Integr. Zool. 7 (2012) 61–73. https://doi.org/10.1111/j.1749-
1253   4877.2011.00279.x.
1254   [43] M.B. Ponczek, M.Z. Bijak, P.Z. Nowak, Evolution of Thrombin and Other
1255   Hemostatic Proteases by Survey of Protochordate, Hemichordate, and

55

1256 Echinoderm Genomes, J. Mol. Evol. 74 (2012) 319–331.
1257 https://doi.org/10.1007/s00239-012-9509-0.
1258 [44] Y. Takada, X. Ye, S. Simon, The integrins, Genome Biol. 8 (2007) 215.
1259 https://doi.org/10.1186/gb-2007-8-5-215.
1260 [45] Z. Wang, C. Li, R. Xing, Y. Shao, X. Zhao, W. Zhang, M. Guo, β-Integrin
1261 mediates LPS-induced coelomocyte apoptosis in sea cucumber *Apostichopus*
1262 *japonicus* via the integrin/FAK/caspase-3 signaling pathway, Dev. Comp.
1263 Immunol. 91 (2019) 26–36. https://doi.org/10.1016/j.dci.2018.10.004.
1264 [46] R.P.A. Wallin, A. Lundqvist, S.H. Moré, A. Von Bonin, R. Kiessling, H.-G.
1265 Ljunggren, Heat-shock proteins as activators of the innate immune system,
1266 Trends Immunol. 23 (2002) 130–135. https://doi.org/10.1016/S1471-
1267 4906(01)02168-8.
1268 [47] H. Zhao, H. Yang, H. Zhao, M. Chen, T. Wang, The molecular characterization
1269 and expression of heat shock protein 90 (Hsp90) and 26 (Hsp26) cDNAs in sea
1270 cucumber (*Apostichopus japonicus*), Cell Stress Chaperones. 16 (2011) 481–
1271 493. https://doi.org/10.1007/s12192-011-0260-z.
1272 [48] E.E. Battin, J.L. Brumaghim, Antioxidant Activity of Sulfur and Selenium: A
1273 Review of Reactive Oxygen Species Scavenging, Glutathione Peroxidase, and
1274 Metal-Binding Antioxidant Mechanisms, Cell Biochem. Biophys. 55 (2009) 1–23.
1275 https://doi.org/10.1007/s12013-009-9054-7.
1276 [49] H. Ba, F. Yao, L. Yang, T. Qin, H. Luan, Z. Li, X. Zou, L. Hou, Identification and
1277 expression patterns of extracellular matrix-associated genes fibropellin-ia and
1278 tenascin involved in regeneration of sea cucumber *Apostichopus japonicus*,
1279 Gene. 565 (2015) 96–105. https://doi.org/10.1016/j.gene.2015.03.071.
1280 [50] K. Mehta, U. Shahid, F. Malavasi, Human CD38, a cell-surface protein with
1281 multiple functions, FASEB J. 10 (1996) 1408–1417.
1282 https://doi.org/10.1096/fasebj.10.12.8903511.
1283 [51] L. Cerenius, K. Söderhäll, Immune properties of invertebrate phenoloxidases,
1284 Dev. Comp. Immunol. 122 (2021) 104098.
1285 https://doi.org/10.1016/j.dci.2021.104098.
1286 [52] J. Jiang, Z. Zhou, Y. Dong, H. Sun, Z. Chen, A. Yang, S. Gao, B. Wang, B.
1287 Jiang, X. Guan, Phenoloxidase from the sea cucumber *Apostichopus japonicus*:
1288 cDNA cloning, expression and substrate specificity analysis, Fish Shellfish
1289 Immunol. 36 (2014) 344–351. https://doi.org/10.1016/j.fsi.2013.12.001.
1290 [53] Z. Wang, X. Fan, Z. Li, L. Guo, Y. Ren, Q. Li, Comparative analysis for immune
1291 response of coelomic fluid from coelom and polian vesicle in *Apostichopus*
1292 *japonicus* to *Vibrio splendidus* infection, Fish Shellfish Immunol. Rep. 4 (2023)
1293 100074. https://doi.org/10.1016/j.fsirep.2022.100074.
1294 [54] S. Zhuang, L. Kelo, J.B. Nardi, M.R. Kanost, An Integrin-Tetraspanin Interaction
1295 Required for Cellular Innate Immune Responses of an Insect, *Manduca sexta*, J.
1296 Biol. Chem. 282 (2007) 22563–22572. https://doi.org/10.1074/jbc.M700341200.
1297 [55] K. Yu, X. Zhao, Y. Xiang, C. Li, Phenotypic and functional characterization of
1298 two coelomocyte subsets in *Apostichopus japonicus*, Fish Shellfish Immunol.
1299 132 (2023) 108453. https://doi.org/10.1016/j.fsi.2022.108453.
1300

1301

1302

1303